Kinematics of subduction in the Ibero-Armorican arc constrained by 3D microstructural analysis of garnet and pseudomorphed lawsonite porphyroblasts from Ile de Groix (Variscan belt)

Domingo G.A.M. Aerden[a,b]
Alejandro Ruiz-Fuentes[a]
Mohammad Sayab[d]
Aidan Forde[c]

[a]Departamento de Geodinámica, Universidad de Granada, Spain
[b]Instituto Andaluz de Ciencias de la Tierra, CSIC/Universidad de Granada, Spain
[c]Saorgus Energy Ltd, Kerry, Ireland
[d]Geological Survey of Finland, Espoo, Finland

Abstract

The small island of Groix in southern Brittany, France, is well known for exceptionally well preserved outcrops of Variscan blueschists, eclogites and garnetiferous micaschists that mark a Late-Devonian suture between Gondwana and Armorica. The kinematics of polyphase deformation in these rocks is reconstructed based on 3D microstructural analysis of inclusion trails within garnet and pseudomorphed lawsonite porphyroblasts using differently oriented thin sections and X-ray tomography. Three sets of inclusion trails striking NE-SW, NNW-SSE and WNW-ESE are recognized and interpreted to witness a succession of different crustal shortening directions orthogonal to these strikes. The curvature sense of sigmoidal- and spiral-shaped inclusion trails of the youngest set is shown to be consistent with north-west- and northward subduction of Gondwana under Armorica, provided that these microstructures developed by overgrowth of actively forming crenulations without much porphyroblast rotation. Strongly non-cylindrical folds locally found on the island are reinterpreted as fold-interference structures instead of having formed by progressive shearing and fold-axes reorientation. Six samples of a lower-grade footwall unit of the Groix ophiolitic nappe (Pouldu schists) were also studied. Inclusion trails in these rocks strike E-W, similar to the youngest set recognized on Groix island. They record Carboniferous N-S shortening during continental collision. These new microstructural data from southern Brittany bear a

strong resemblance to earlier measured inclusion-trail orientations in the north-western Iberia Massif. A best fit between both regions suggest about 20° clockwise rotation of Iberia during the Cretaceous opening of the Gulf of Biscay.

Key words: porphyroblast inclusion trails, FIA, Variscan subduction, Ibero-Armorican arc, Ile de Groix, Iberia rotation.

1. Introduction

Structural analysis in metamorphic terrains is traditionally based on a combination of geological mapping, study of structures in outcrops and microstructures in thin sections that are commonly cut parallel to the stretching lineation aimed at determining a shear sense. Not rarely does this approach produce ambiguous or even paradoxical results (e.g. Zhang & Fossen, 2020), apart from not allowing access to the kinematics of strongly overprinted early-formed fabrics. A major breakthrough in this state of affairs was claimed by Bell et al., (1985, 1986) and Bell & Johnson (1989) after recognizing the polyphase origin of inclusion-trail patterns that were previously assumed to have formed by progressive shearing and porphyroblast rotation (e.g. Zwart, 1960; Spry, 1963; Rosenfeld, 1970). Sigmoidal and spiral-shaped inclusion trails were reinterpreted as representing multiple crenulations that became sequentially fixed within non-rotating porphyroblasts with episodic growth histories. The lack of porphyroblast rotation would have resulted from the general micro-partitioning of deformation between cleavage planes (accommodating shear-strain components) and microlithon domains, and the preferential nucleation of porphyroblasts within the latter (Bell et al., 1985; Aerden, 1995; Fay et al., 2008). Axes of inclusion-trail curvature in this view are not controlled by shearing directions but by the intersection of 2 or more foliations causing crenulation and folding, and consequently referred to as 'Foliation-Intersection/Inflexion Axes' abbreviated as 'FIA' (Bell et al., 1992; Bell et al., 1995; Stallard et al., 2003). Another major difference with the classic model, is that the curvature sense (clockwise / anticlockwise) of inclusion-trails being determined by the (S- or Z) asymmetry of overgrown crenulations indicates an opposite shear sense as would have been originally deduced (see Fig. 1a, b).

The above conceptual changes regarding the significance of porphyroblast inclusion trails prompted extensive collection of orientation data for these microstructures in various metamorphic belts, which revealed their regional-scale consistency and close relationship to

large-scale tectonic processes (e.g. Bell et al., 1998; Bell & Welch, 2002; Sayab, 2005; Ali, 2010; Shah et al., 2011; Aerden, 1994, 1998, 2004, 2013; Kim & Ree, 2013; Abu-Sharib & Bell, 2011; Abu-Sharib & Sanislav, 2013; Aerden & Sayab, 2017). The methodological novelty of this research resides in the integration of quantitative microstructural data derived from precisely oriented thin sections of different samples in an external (geographical) reference frame. For this purpose, thin-sections are systematically cut in fixed orientations relative to geographic coordinates, independent of the (variable) orientations of the macroscopic lineation and foliation in each sample. Vertical and/or horizontal thin section orientations are usually chosen as these represent small-scale true cross-sections and maps that can be directly compared with their larger-scale equivalents.

Aerden (2004) pioneered this approach in NW-Iberia where he distinguished 4 sets of inclusion-trails, each with a specific and regionally consistent trend. The E-W trend of the oldest set was interpreted to record N-S directed compression and subduction with unknown polarity. This was followed by several changes in the direction of crustal shortening that produced the 3 younger inclusion-trail sets. The youngest two sets, trending NE-SW and WNW-ESE respectively, were shown to correlate with regional-scale fold-interference patterns developed throughout the Iberian Massif and this was key to the discovery of the partially blind Central Iberian Arc (Aerden, 2004; Martinez Catalán et al., 2009).

In this paper we report a similar microstructural study in the Armorican Massif focusing on high-pressure metabasites of Ile de Groix, but also paying attention to a lower-grade footwall unit known as the Pouldu schists. The island of Groix (ca. 15 km^2) is a national reserve famous for exceptionally well preserved coastal outcrops of Variscan blueschists, eclogites and interlayered garnetiferous micaschists (Audren et al., 1993). These are generally accepted to represent the remains of the floor of a narrow ocean that, in the late Silurian and lower Devonian, separated Gondwana in the south from the Armorica microplate to the north. Closure of this ocean by subduction of the margin of Gondwana produced high-pressure metamorphism dated 370-360Ma on Ile de Groix (Bosse et al., 2005). In NW-Iberia, a similar ophiolitic unit is recognized and correlated with the one exposed on Groix island (Arenas et al., 1995; Diaz-García et al., 1999; Ballèvre et al., 2009, 2015).

The polarity and kinematics of ophiolite emplacement have remained poorly constrained by (micro)structural data. Indeed, not much appears to have changed since Quinquis et al. (1978) wrote: "*the bulk sense of shear on Groix has not yet been determined unequivocally, but may perhaps be deduced from systematic analyses of fold asymmetry and of microstructures in and around syntectonic garnets. The significance of glaucophane*

orientation in the basic rocks of Groix also needs to be studied: the orientation is extremely variable and may not be simply related to a shear direction." Precisely along these lines of suggested further research, we have performed detailed 3D microstructural analyses of 10 garnetiferous blueschist samples of the Ile de Groix ophiolitic nappe, 4 samples of albite-porphyroblast bearing greenschists (Pouldu schists) of a footwall unit cropping out along the mainland coast, plus 2 kyanite-staurolite schists collected further inland from the North-Armorican Zone (Fig. 2). Integrated with structural field data from previous workers, the new microstructural data indicate a polyphase deformation history masked by a seemingly simple L-S fabric. Implications for the formation mechanism of sheath folds (Ile de Groix is one of the main type locations) are discussed, and for variations in the direction of Variscan subduction with time. A possible correlation is proposed between inclusion-trail trends in NW-Iberia and in the Armorican Massif, which if correct, implies 20° anticlockwise rotation of Iberia during opening of the Gulf of Biscay.

2. Geological setting and previous work

The Variscan (or Hercynian) orogeny took place in the Devonian and Carboniferous as a consequence of Gondwana-Laurussia convergence with the Armorica and Avalonia microcontinents occupying intermediate positions (e.g. Matte, 2001). The resulting closure of oceanic domains created multiple ophiolitic sutures, whose precise location, timing and correlation continues to be a major research topic (e.g. Azor et al., 2008; Faure, 2008; Ballèvre et al., 2009; Arenas et al., 2016). The high-pressure rocks of Ile de Groix are part of a partially submerged ophiolitic klippen of a thrust nappe that separates Armorican crustal units in the hangingwall (outcropping in the Central- and North-Armorican Domains) from Gondwana derived units in the footwall cropping out extensively in the South Armorican Domain and NW Iberia (Fig. 2). Mineral and stretching lineations have an average N-S trend in the east and south-east of the island, changing gradually to NW-SE further north and west. Bosse et al. (2002) proposed a thrust contact between garnetiferous eclogites, blueschists and micaschists outcropping in the eastern part of the island (Fig. 3a), overlying lower-grade (albite-epidote facies) unit outcropping in the west containing scarce garnet porphyroblasts (Triboulet, 1974; Schulz, 2001). Peak metamorphic conditions are estimated at 475°C/18-20kbar in the upper unit and 450°C/12-15kbar in the lower unit (Bosse et al. 2002; Ballèvre et al., 2003).

The general tectono-metamorphic zonation of the Armorican Massif has led most workers to accept a north-dipping subduction zone associated with south verging thrusting (e.g. Matte, 2001; Faure et al., 2008; Ballèvre et al., 2009; Ballèvre 2015; Philippon et al., 2009; Fig. 2b). However, structural data have not allowed to independently confirm this and, in fact, have yielded conflicting results. Lagarde (1980) concluded NW directed thrusting from shear criteria in the Champtoceaux Complex (Fig. 2a) suggesting south-east directed subduction. A similar kinematic was deduced on Ile de Groix from rotated snowball garnets and quartz c-axes fabrics by Quinquis (1980), Quinquis & Choukroune (1981) and Cannat (1985). To reconcile this with north-dipping subduction, Quinquis & Choukroune (1981) proposed that this shear sense corresponds to back-thrusting and ophiolite obduction, but little independent evidence has been presented to support this model.

Quinquis (1980) noticed that shear bands (C and C' planes) on Ile de Groix indicate opposite shear senses that could not be clearly linked to different metamorphic conditions and were therefore interpreted as conjugate sets. Shelley and Bossière (1999) endorsed this and showed that quartz fabrics studied in 57 samples also record about equal amounts of opposite shear-senses. From this they concluded that the main foliation and lineation of Ile de Groix formed by coaxial vertical shortening in a period of crustal extension and exhumation. In contrast, Philippon et al. (2009) recently argued a consecutive origin of a first set of top-to-the-SW shear bands related to prograde metamorphism, followed by a second top-to-the-north set during retrogression. However, they did not resolve the conflict this poses with respect to top-to-the-north shearing indicated by 'rotated' garnets, which clearly formed during prograde metamorphism (Bosse et al, 2002; Ballèvre et al., 2003).

3. Microstructural analysis using vertical and horizontal thin sections

A total of 138 oriented thin sections were studied of 33 oriented samples: 20 from Ile de Groix, 9 from the Pouldu schists and an equivalent unit in the Baye d'Audièrne (Tréogat formation), and 4 from the Central Armorican Zone (Fig. 2). Their precise location can be consukted in the electronic supplement provided with this paper. Initially, a single horizontal thin section was cut of each to evaluate the interest of the rock for further study and to measure the strike of inclusion trails (relative to geographic coordinates). The latter only proved possible in about half of the samples, as the other half contain garnets or plagioclase porphyroblasts that are too altered or have poorly developed inclusion trails. Seven Ile de Groix samples containing the most promising inclusion trails were studied further in 6 vertical

thin sections striking N0, N30, N60, N90, N120 and N150 aimed at constraining the orientation of inclusion-trail curvature axes (i.e. 'FIA'; see Introduction) and record their curvature sense.

3.*1. Strike of inclusion trails in Ile de Groix blueschist samples*

Inclusion-trail strikes were measured in garnet porphyroblasts of 10 samples from 3 areas of Ile de Groix, all pertaining to the high-grade eastern domain of the island or 'upper unit' of Bosse et al. (2002; Fig. 3a). The data are plotted in moving-average rose diagrams (Fig. 3b) made with the computer program 'MARD' of Munro & Blenkinsop (2012). As pointed out by these authors, moving-average rose diagrams reveal the distribution of modal maxima more accurately than their conventional binned equivalents.

Stretching lineations in the high-grade domain are associated with a gently dipping or subhorizontal composite foliation. Therefore, if porphyroblasts rotated in the direction of the lineation during growth, then they can be expected to have developed inclusion trails broadly striking orthogonal to that lineation (Fig. 1a). Our measurements, however, show exactly the opposite: a main NNE-SSW maximum subparallel to stretching lineations and fold axes (Fig. 1c). This agrees better with a 'non-rotational' origin of inclusion trails via overgrowth of successive crenulations, and this is supported further by truncational relationships commonly seen between inclusion trails in porphyroblast cores versus rims (Fig. 4a and b). Automatic orientation analysis of the inclusion-trail patterns pictured in these Figures using the image analysis software package *Fiji* (Schindelin et al., 2012), reveals their bimodal preferred orientations reminiscent of the subvertical and subhorizontal preferred orientations of inclusion-trails previously reported in other metamorphic regions (e.g. Bell et al., 1992; Hayward, 1992; Aerden, 1994, 1998, 2004; Mares, 1998; Stallard & Hickey, 2001; Bell & Sapkota, 2012; Sayab, 2005; Shah et al., 2009; Aerden and Ruiz Fuentes, 2020). These authors all interpreted this to reflect alternations between orogenic shortening and gravitational collapse, but a somewhat different explanation will be proposed in section 4.4 based on additional 3D data obtained by X-ray tomography.

3.2. Inclusion-trail curvature sense and genetic implications

Quinquis & Choukroune (1981) reported that out of a total of 29 thin sections studied (presumably all cut parallel to the stretching lineation), 26 contained sigmoidal or spiral-

shaped inclusion trails indicating top-to-the north shearing. Since these authors assumed the 'rotational' inclusion-trail model, it follows that the trails predominantly curve anticlockwise when viewed in westward direction. In effect, we found the same predominance in our samples after counting the number of clockwise vs. anticlockwise trails in all vertical thin sections striking N-0, N30, N120 and N150, that is, in all thin sections making a small angles with the regional stretching lineation. This resulted in 99 anticlockwise and 27 clockwise inclusion trails viewing westward — a ratio of about 4:1. The classic 'rotational' interpretation of inclusion trails predicts top-to-the-north shearing from this asymmetry, which is paradoxical with respect to the widely accepted northward subduction and southward thrusting in the Armorican Massif. The 'non-rotational' model resolves this paradox as it predicts an opposite shear sense from the same inclusion-trail asymmetry, consistent with top-to-the south thrusting (Bell & Johnson, 1989; their Figs. 16 and 17).

3.*3. Average FIA trends in 5 Ile de Groix samples*

Hayward (1990) devised a method for determining the average orientation of porphyroblast FIAs in a sample. The method exploits the fact that sigmoidal or spiral-shaped inclusion trails, just like asymmetric folds, either exhibit an S- or Z-asymmetry in cross-section (thin-section) depending on the orientation of the section relative to the FIA. First, a radial set of vertical thin sections is cut from the sample with regular angular spacing around the compass. From these, the average FIA trend can be constrained to the strike interval where the inclusion-trail asymmetry observed in the different thin sections switches (e.g. Abu-Sharib & Sanislav, 2013 - their Fig. 2). Once the average FIA trend is known, the average FIA plunge can be constrained from by cutting a new radial set of thin-sections, this time about a horizontal axes oriented orthogonal to the FIA trend. The method was refined by Bell et al. (1995) to potentially allow the distinction of multiple FIA sets in a sample with different timing.

We successfully applied the method to 5 samples whose average FIAs are represented in Fig. 3b as pie-cake symbols. FIAs were constrained to within 30°, but 10° for sample G7 thanks to cutting 2 extra thin sections. The plunge direction could also be determined from the asymmetry of inclusion trails as seen in horizontal thin sections, but we did not determine plunge angles because of the large amount of extra thin sections needed. No results were obtained for samples G18, G19 and G20 as these contain relatively few porphyroblasts whose inclusion trails show inconsistent asymmetries in most of their thin sections. X-ray

tomography data for G20 presented in section 4.6. suggest that this inconsistency is due to a mixture of 2 different FIA sets in these samples that could not be resolved using thin sections. Samples G3, G13 and G15 mostly contain garnets with straight inclusion trails and too few asymmetric ones to confidently apply the technique.

3.*4. Mainland samples (Pouldu schists, Tréogat formation, Central Armorican Domain)*

The 'Pouldu schists' are a volcano-sedimentary unit metamorphosed in greenschist- to amphibolite-facies conditions (380-650°C/5.5-6.5kbar; Triboulet, 1992). They crop out in a ca. 50 km long band along the southern coast of Brittany and contain abundant albite porphyroblasts (Fig. 2). The macroscopic cleavage in the field strikes E-W to NE-SW and generally dips steeply north or south. Horizontal thin sections of 7 oriented samples of the unit show a N060 striking foliation cut by widely spaced E-W striking dextral shear bands, likely related to the south Armorican shear zone system. In sample PO5, the N060 striking main foliation has the appearance of a narrowly spaced crenulation cleavage overprinting an older more E-W striking foliation.

The strike of inclusion-trails in albite porphyroblasts were measured in 3 greenschist samples of the Pouldu schists (PO2, PO3, PO5) and in a fourth sample (AU1) of similar rocks cropping out in the Baye d'Audièrne (Tréogat Formation; Luck et al., 2002). Inclusion trails consistently strike E-W to ESE-WNW in PO2, PO3, and PO5, but have a larger spread in AU1 (Fig. 3b). N-S striking vertical thin sections of PO2 and PO3 show that the main foliation ('S2' in Fig. 5a) crenulates an older 'S1' included in syn-D2 porphyroblasts (Fig. 5b). Some later porphyroblast growth, probably linked to the development of weak subhorizontal crenulations ('S3' in Fig. 5), created younger inclusion trails of 'S2' (Fig. 5b). Nearby granites dated 330-320Ma are deformed by 'S2' (Béchennec et al., 2012) and imply that this cleavage post-dates the Late-Devonian to early Carboniferous metamorphism and associated polyphase deformation of Ile de Groix (365-345Ma; Bosse et al., 2005).

Two staurolite-kyanite schists from the Central Armorican Domain collected about 5km NNE of Quimper were studied in horizontal thin sections only. Their inclusion trails strike broadly N060 (Fig. 3d) and might correlate with the equally N060 striking 'S2' in our Pouldu Schist samples. The age of metamorphism in these rocks is broadly constrained to the period 350-320Ma (Schulz et al., 1998).

4. X-ray tomography of 5 Ile de Groix samples

272

273 4.*1. Data acquisition and processing method*

274

275 X-ray computed tomography (XCT) scans were acquired at the University of Granada
276 with an Xradia 510 (Versa Zeiss) microtomographer at resolutions of 13-15 um, using 140kV
277 voltage and 2500-3200 projections. Four thin-section blocks, each measuring 10-15 cm^3, were
278 scanned of samples G3, G11, G12, and G14 plus a more irregular piece of G20 of similar
279 volume. Geographic orientation arrows made of metal wire were stuck on the samples to aid
280 reorientation of the generated Tiff image-stacks such that geographic north is parallel with the
281 Y-axes, and true vertical with the Z-axes. Image stacks were processed with the Fiji software
282 package (Schindelin et al., 2012). After reorientation, the spatial orientation of all straight
283 inclusion-trails or inclusion-trail segments visible in the image stacks were determined by
284 measuring their strike and pitch angles on XY-, YZ- and XZ-slices and fitting those angles to
285 great circles on a stereonet. Furthermore, the curvature axes of individual sigmoidal or spiral-
286 shapes inclusion-trails (FIA) were measured in analogous manner as the thin-section-based
287 technique of Hayward (1990; see section 3.3), and as previously done by Huddlestone-
288 Holmes & Ketcham (2010), Aerden & Ruiz-Fuentes (2020) and Sayab et al., (2021). First,
289 the FIA trend is constrained by interactively rotating a vertical slice through the porphyroblast
290 and recording where the inclusion-trail curvature sense switches. Then, a horizontal slice is
291 interactively rotated about a horizontal axes oriented normal to the previously determined FIA
292 trend to constrain the FIA plunge.

293 The image stacks also allowed us to study the preferred orientation of garnet
294 porphyroblasts as well as relatively large opaque minerals present in all 5 samples. The BoneJ
295 plugin of *Fiji* (Doube et al., 2010) was used for this purpose. This tool enables automatic
296 calculation of best-fit ellipsoids for a large number of 'objects' in a binary (black & white)
297 image stack. To apply this, X-ray scans were first segmented by thresholding, only leaving
298 voxels with grey-scale values within the range corresponding to garnet crystals or opaque
299 minerals, and then binarizing the stack (i.e. setting all grey values to black). Subsequently, a
300 size-filter was applied to remove small particles and in some cases the 'dilate' tool to re-join
301 'objects' belonging to the same garnet crystal that became separated during thresholding due
302 to the presence of fractures and related alteration. In all samples except G20, well developed
303 preferred orientations of opaque minerals were detected, but not of garnets. In G20, an
304 opposite situation was found: well preferred orientation of garnets only. In the following
305 subsections microstructural results are described for each sample and presented in stereoplots

made with the program 'Stereonet' of R. Allmendinger. The original files of these stereoplots are provided in the electronic supplement.

4.*2. Sample G11*

G11 is a blueschist from 'Amer' in the SE of the island (Fig. 3a). It contains garnet porphyroblasts as well as rectangular pseudomorphs probably after lawsonite composed of a mixture of white mica, chlorite, albite and epidote (Cogné et al., 1966; Felix & Fransolet, 1972; Ballèvre et al., 2003). Lawsonite relics have never been found, though, and some authors have argued that the replaced mineral could have been plagioclase (Shelley & Bossière, 1999). Lawsonite, is a high-pressure mineral and should have grown partially synchronous with garnet on a prograde path, whereas plagioclase is more likely to have formed during retrogression. Thus, the relative timing of the pseudomorphed mineral relative to garnet growth and inclusion trails is highly relevant to this question.

Inclusion trails in garnet porphyroblasts of G11 vary from simple to sigmoidal to spiral-shaped, but never curve more than about 90° from the centre to the rim (Figs. 6a, b, c, g and 6). The tomographic images further revealed the presence of relatively large elongate crystals with high X-ray attenuation (higher than garnet), which in thin section were identified as magnetite, partially or completely replaced by brown-reddish goethite (Fig. 6d, h). Some of the opaques attain porphyroblastic sizes and contain scarce silicate inclusions. Best-fit ellipsoids calculated for these crystals with *BoneJ* (see section 4.1.) have long-axes (X) well aligned with the macroscopic mineral/stretching/intersection lineation, and short axes normal to the foliation (Fig. 7).

Sigmoidal- or spiral-shaped inclusion trails were measured both in the centre and in the rims, where they become sharply deflected or truncated by younger inclusion trails. The porphyroblast-rim measurements tightly define a steeply SW dipping plane, whereas foliations within porphyroblast cores have more variable orientations between steeply NE-dipping to shallowly W-dipping. The intersection lines of core- and rim inclusion-trail planes agree well with 10 FIAs measured directly with the asymmetry-switch technique described in the previous section. Simple (straight) inclusion trails have variable orientations that broadly coincide with the foliations measured in porphyroblast cores and rims associated with sigmoidal and spiral-shaped trails.

The above data allow confident interpretation of the bimodal inclusion-trail strike pattern exhibited by the rose diagram for G11 in Fig. 3b as corresponding to 2 age sets of

inclusion trails: an older set striking NNW-SSW and a younger one striking WNW-ESE. Note that the 10 individual porphyroblast FIAs determined from the X-ray scan agree well with the average FIA initially determined from the radial set of thin sections (Fig. 3b).

Some of the lawsonite pseudomorphs in G11 also have visible inclusion trails in the X-ray scan (Fig. 6e, f, and h), although less finely defined as in garnets. They are straight to weakly sigmoidal, oblique to the matrix foliation, but subparallel to inclusion trails in garnet-rims. The latter suggests that the pseudomorphed mineral grew synchronous with late-stage garnet and this supports that the pseudomorphed mineral was lawsonite and grew towards the end of the prograde path as concluded by Ballèvre et al. (2003). Interestingly, the curvature sense of inclusion trails in the pseudomorphs is mostly opposite to that in garnets when viewed in N-S vertical sections. Assuming a 'non-rotational' origin of the trails, this implies a change from top-to-the-south shearing to top-to-the-north shearing that is further discussed in section 6.3.

4.*3. Sample G12*

G12 is a similar blueschist as G11 from the same outcrop, but only one possible lawsonite pseudomorphs could be identified in the X-ray scan which does not show an internal fabric. The tomography of this sample reveals an early NNW-SSE striking foliation preserved within garnet porphyroblasts, overprinted by a steeply S-dipping foliation included in some garnet rims (Fig. 7). The garnet-rim foliation is in turn deflected or truncated by a subhorizontal crenulation cleavage in the matrix that is responsible for the flat-lying macroscopic cleavage. The same opaque minerals as found in G11 are present in the matrix, but now also as relatively large inclusions inside garnets, often occupying a central position suggesting that the garnets nucleated on those grains. Best-fit ellipsoids for the matrix opaques demonstrate their strong elongation in NW-SE direction parallel to the macroscopic lineation, and parallel to the strike of inclusion trails in garnet.

The above data allow to correlate the different peaks in the strike rose diagrams for G11 and G12 in Fig. 3b as (i) an early NE-SW striking foliation preserved in the cores of spiral-shaped inclusion trails, (ii) a younger NNW-SSE striking foliation included in the cores of sigmoidal inclusion trails with variable dip angles, and (iii) a still younger ESE-WNW foliation preserved in garnet rims and in lawsonite pseudomorphs.

4.*4. Sample G14*

G14 is another blueschist from Amer containing numerous relatively small (1-2 mm) garnets with straight, sigmoidal or spiral-shaped inclusion-trails. The spiral patterns exhibit significantly greater curvature (up to 180°; Fig. 4b) as in G11 and G12. Unfortunately, only a few garnets had visible inclusion trails in the tomography because of their very fine grain size and profuse fracturing of garnets. A few inclusion-trail planes could be measured plus 5 FIAs plunging steeply in different directions (Fig. 8a).

Opaque crystals are elongated in N-S to NE-SW direction parallel to the modal maximum defined by 62 inclusion-trail strikes measured in 2 horizontal thin sections (Fig. 3b). A cm-scale fold outlined by an epidote-rich layer was found, whose axial plane also strikes NW-SE (Fig. 8a), hence suggesting a genetic relationship with the inclusion trails. Vertical sections oriented at a high angle to the fold axes (Fig. 8c) show refolding with subhorizontal axial planes related to the subhorizontal crenulation cleavage observed in thin sections of sample G7 (Fig. 4a). In plan view, the fold is transected by N-S striking cleavage zones and quartz lenses (Fig. 8d).

Based on their orientations, the 5 measured inclusion-trail planes can be correlated with the 3 sets already distinguished in G11 and G12. That is: (i) an early NE-SW set responsible for the strike maximum of 62 inclusion-trails measured in 2 horizontal thin sections of G14 (Fig. 3b), (ii) a NNW-SSE striking set, and (iii) a late WNW-ESE set. The lack of subhorizontal internal foliations in G14 or in any other of the samples studied with X-ray tomography implies that the roughly bimodal distribution of pitch angles of inclusion-trails in G7 and G14 (Fig. 4c) does not reflect a succession of subvertical and subhorizontal foliations associated with compression-collapse cycles as shown in other metamorphic regions (Aerden & Ruiz Fuentes, 2020 and references cited therein). but rather two sets of moderately to steeply dipping foliations with different strikes.

4.5. *Sample G3 and G7*

G3 was collected close to Fort Nosterven on the east-coast of the island, about 1 km south of G7. Garnets in this glaucophane-epidote schist have well developed straight and sigmoidal inclusion trails, whose strikes were measured in horizontal thin sections. The average N020 FIA trend in G7 was determined from 8 vertical thin sections with different strikes. G3 was studied further with X-ray tomography, but its inclusion trails are poorly visible in the scan. The few that could be measured all dip steeply NW with N020 strike,

parallel to the average FIA in sample G7 and a set of gently SSW plunging folds measured by C. Audren near G7 at Pelage du Trech (1974, unpublished data; Fig. 9b). A single porphyroblast FIA was also measured, defined by sigmoidal inclusion trails that curve into a subvertical N120 striking position in the porphyroblast rim. It is most likely related to one of Audren's fold axes which has an anomalous N120 trend. Thus, this fold axes is probably younger as the main group of SSW trending fold axes. All the above described data are consistent with the orientations and relative timing of 3 main sets of inclusion trails and related macroscopic structures in Ile de Groix, coded pink, blue and orange in our Figures.

4.*6. Sample G20*

G20 was collected near Port Lay on the central-north coast of Groix (Fig. 3a). The macroscopic cleavage dips 50° NE here and is associated with a subhorizontal mineral lineation parallel to small-scale tight to isoclinal fold axes. Six garnet FIAs defined by sigmoidal inclusion trails were measured using X-ray tomography plus a larger number of straight inclusion trail planes. Five FIAs plunge moderately NE and are caused by the intersection of an older set of NE-SW striking subvertical inclusion trails with a younger set of steeply NE- or SW-dipping ones. Again, this allows both sets to be correlated with similarly striking inclusion trails in the other samples (Fig. 3b). The macroscopic cleavage is conspicuously parallel to a subset of the younger (NNW-SSE striking) inclusion-trails suggesting a genetic relationship. The sixth FIA that was determined plunges shallowly SSE and probably formed after the others by overgrowth of the younger inclusion trail set (blue great circles in Fig. 9c).

Abundant opaque minerals in the sample conspicuously cluster around garnet crystals but ellipsoid best-fitting did not reveal significant preferred orientations. Axial ratios of the opaques are also much lower as in the earlier described samples (2.0 versus 4.0). Best-fit-ellipsoids for garnet porphyroblasts, however, revealed their preferred elongation parallel to the lineation and fold axes and an average axial ratio of 2.1 (Fig. 9c). Aerden & Ruiz-Fuentes (2020) recently showed that garnets commonly grow elongate either parallel or perpendicular to their FIAs due to preferential nucleation in actively forming microlithon domains and growth controlled by the pre-existing cleavage within these domains. The 6 FIAs measured in G20 are all approximately normal to the maximum elongation axes (X_Gt) of their host garnets (Fig. 9c).

5. Tectonic interpretation

5.1. Changes in subduction direction

Evidence has been presented for 3 regionally developed sets of inclusion-trails with consistent orientations that successively developed in blueschist-eclogite facies rocks of Ile de Groix. All 3 sets probably formed on a single prograde metamorphic path reaching 18–20 kbar, 450 °C according to detailed petrological work (Bosse et al. 2002; Ballèvre, 2003). Schulz et al, (2001), however, proposed a superposition of 2 (Variscan) metamorphic cycles based on complex chemical zoning in amphiboles, whose relationship with the different generations of inclusion trails distinguished herein merit further research.

The 3 sets of inclusion trails have moderate to subvertical orientations and can be linked to three periods of crustal shortening perpendicular to their NE-SW, NNW-SSE and WNW-ESE strikes. The earlier mentioned predominance of anti-clockwise inclusion trails observed in thin vertical thin sections that strike parallel to or at a low angle with the regional mineral lineation is likely determined by the oldest (NE-striking) and youngest (E-W striking) inclusion-trail sets as these intersect the thin section planes at a high angle. The intermediate-age inclusion trail set strikes subparallel to the regional mineral lineation and hence can be expected to produce inconsistent curvature senses in the same thin sections (cf. Hayward, 1990). This may be why about 25% of all counted porphyroblasts exhibit an opposite curvature sense (i.e. clockwise).

Consequently, we interpret the oldest NE-SW striking inclusion trails to witness a NW directed subduction. The polarity of an intermediate subduction stage, corresponding to NNE-SSW striking inclusion trails, remains undetermined by our data, but was probably towards the WSW according to other geological evidence (e.g. Martinez Catalán et al., 1997). The asymmetry of the youngest WNW-ESE striking trails correspond to the latest stages of subduction in northward direction, followed by exhumation. Inclusion trails in the Pouldu schists have a similar orientation as the youngest set of Ile de Groix (see section 3.4.). They record continued N-S compression in the Carboniferous that still generated a late set of post-metamorphic chevron-type folds with E-W trending axes on Ile de Groix (see section 6.1.).

5.2. A gravitational spreading high-grade thrust nappe?

The average dip of all 103 inclusion-trail planes measured with X-ray tomography in 5 samples from Ile de Groix is 57° (σ=21°). The average plunge of all 33 measured FIAs is 43° (σ=15°). These relatively steep dips and plunges imply a limited role, if any, of intermittent gravitational collapse stages during prograde metamorphism. This is because compression-collapse cycles should generate subhorizontal FIAs formed by the intersection of alternating subvertical and subhorizontal foliations. This situation has been shown in the Appalachians, the European Alps (Bell & Bruce, 2006; their Fig. 18) and Variscan NW-Iberia (Aerden, 2004; his Fig. 4b). The inclusion trails of Ile de Groix, however, formed in the context of a Late-Devonian subduction, before continental collision could have sufficiently thickened the crust to start-off gravitational collapse phases.

A notable difference between eastern and western Ile de Groix, apart from the higher-metamorphic grade of the former, is the attitude of the main foliation. This is particularly clear from structural data of Cogné et al. (1966) compiled and re-plotted in Fig. 10a. Whereas in eastern Groix, the main foliation dips gently east to south, in the west it dips moderately to steeply NE or SW. This difference was previously attributed to large-amplitude folding of a single main foliation with NW-SE axial planes (see Bosse et al, 2002 - their Fig. 12). We alternatively propose that the flat lying foliation in the high-grade eastern domain is more weakly developed in the lower-grade western domain, where consequently, older foliations and folds are more widely preserved as shown conceptually in Fig. 10b. This model is consistent with the extrusion and gravitational spreading of a thrust nappe over a lower-grade footwall (Fig. 10b) as famously modelled by Bucher (1956) and Merle (1989) and as proposed earlier for thrust nappes in the Montagne Noire (Aerden, 1998; Aerden & Malavieille, 1999). The model accounts for vertical shortening components associated with the flat lying main foliation of the high-grade domain indicated by strain shadows, shear bands and quartz fabrics all showing inconsistent shear senses (Shelley & Bossière, 1999), and by steeply dipping foliations preserved within porphyroblasts documented here.

Detailed field observations of Cogné et al. (1966) and Boudier & Nicolas (1976) at Vallon du Lavoir (central south coast; Fig. 3a) corroborate an important role of vertical shortening also in the lower-grade western domain. Both works describe a decametre-scale upright anticline at this location overprinted by a horizontal crenulation cleavage and related m-scale refolding (Fig. 10c and d). This geometry is directly comparable with the cm-scale vertically flattened fold found in sample G14 (Fig. 8c).

Samples G18, G19 and G20 come the same outcrop near Port Lay (Fig. 3a) where the main cleavage dips steeply (50°) NE, despite still belonging to the high-grade domain and

located close to the inferred basal thrust. The first explanation that comes to mind is that the foliation was originally flat lying but was later steepened by folding. However, the following observations suggest otherwise. Firstly, the foliation is parallel to and partially continuous with a set of NNW-SSE striking inclusion-trails in G20 (Fig. 9c - blue great circles). In contrast, the flat lying transposition cleavage at Amer (samples G11, G12 and G14) formed after a younger set of WNW-ESE striking inclusion trails (Fig. 7 - orange great circles). Thus, the main foliations at both locations do not appear to be the same generation. Secondly, the main foliation in G20 is sharply deflected towards the horizontal at matrix-garnet boundaries suggesting the sample was affected by vertical shortening although only weakly. This leads us to interpret the studied outcrop at Port Lay as forming part of a low-strain lens (Fig 10b).

6. Discussion

6.1. Inclusion trail sets vs. folding sequences in the field

Cogné et al (1966) distinguished 3 deformation phases. Their first phase corresponds to tight to isoclinal folds (called 'fundamental folds') with NW-SE to N-S trends. The second phase caused refolding of the 'fundamental' folds associated with a SW dipping crenulation cleavage striking N130-140 as shown in their field sketch (Fig. 10d). A third set of E-W trending chevron-type folds were considered post-metamorphic. The authors describe variable relationships between a mineral lineation defined by glaucophane and epidote and fold axes as being commonly parallel to each other and apparently coeval, but locally oblique indicating a younger age of the folding, and still elsewhere associated with 2nd-phase folds. In the latter case, 2 sets of oblique glaucophane lineations were reported (their Fig. 12, p 70).

Boudier and Nicolas (1976) distinguished 4 deformation phases (D1-D4), the youngest of which corresponds to the third-phase post-metamorphic structures of Cogné et al. (1966). D1 refers to the mineral-lineation (L_1), D2 and D3 to NNW-SSE trending folds that partially reoriented L_1. Orientation data of these authors show a good match with the strike directions of our successive inclusion trail sets (Figs. 11b, c). However, our new microstructural indicate an opposite relative timing of N165- versus N120-trending fabrics as concluded by Boudier and Nicolas (1976), but in agreement with Cogné et al. (1966) and Quinquis & Choukroune's (1981). Further evidence for younger N120-structures was found in a sketch by made in 1974 by C. Audren (unpublished as far as we know) kept at the 'Maison de la Reserve Naturelle Le

Bail' on Ile de Groix. The sketch, redrafted in Fig. 11a, depicts folding of a N160 trending lineation around the hinge of a N120 fold.

6.2. Formation mechanism of sheath folds

Based on a detailed study of quartz fabrics in 57 samples, Shelley and Bossière (1999) concluded that most folds of Ile de Groix island nucleated with their axes immediately parallel to the maximum stretching direction (X), instead of first parallel to the Y-axes and then rotating towards X during progressive shearing (cf. Cobbold & Quinquis, 1980; Quinquis and Choukroune, 1981). However, they still interpreted a single kinematic frame with a component of shortening parallel to the intermediate strain axes (Y). The polyphase character of the main (composite) foliation and lineation demonstrated herein places the significance of fold-axes parallel stretching and the origin of sheath folds in a different light. Fold axes could have nucleated with their axes parallel to X due to vertical shortening of vertical foliations and upright folds whose axes were already subparallel to X (Fig. 12). Likewise, non-cylindrical folds and condom folds may have formed by vertical flattening of precursor folds with subvertical axial planes but steeply plunging or subvertical axes (Fig. 12). Thus, depending on the geometry of the precursor folds, new folds nucleated either with straight axes parallel to X, or with strongly curved axes oblique to X. This model agrees well with Audren & Triboulet's (1993) analysis of a sheath from Groix that concluded that the fold started to form towards the end of the prograde path but developed further during the retrogression.

6.3. Inclusion trail data vs. shear-bands

Predominantly clockwise curvature of inclusion-trails in lawsonite pseudomorphs studied in sample G11, versus anticlockwise in garnets suggests a change from top-to-the-south to top-to-the-north shearing, provided that the inclusion-trails formed by overgrowth of crenulations (the non-rotation model). Interestingly, Philippon et al. (2009) deduced a similar switch in regional tectonic transport from 2 sets of shear bands studied along the south coast of the island. They claimed that high-grade rocks conserving well-shaped lawsonite pseudomorphs in the south-east of the island only contain top-to-the-south shear bands, whereas rocks lacking such pseudomorphs also contain top-to-the north criteria or exclusively so. Based on this, it was concluded that prograde metamorphism was associated with top-to-

576 the south shearing, and that this was followed by top-to-the-north shearing, retrogression and
577 partial destruction of pseudomorphs. However, our lawsonite-bearing sample G11 cast doubts
578 on this model as it exhibits mainly top-to-the north shear-sense criteria (Fig. 13) despite
579 coming from a location where, according to Fig. 6 of Philippon et al. (2009), top-to-the south
580 criteria should be found. Moreover, the authors excluded from their statistical analysis shear
581 bands occurring close to or within inverted limbs of tight to isoclinal folds perhaps because
582 they assumed that the folding might have overturned the shear bands. In the absence of less
583 ambiguous evidence for different metamorphic conditions of both shear-band sets we
584 consider a synchronous origin of opposite shear-band sets in bulk coaxial deformation
585 accompanied by retrogression more likely following Shelley & Bossière (1999). The local
586 predominance of one set may simply reflect the partitioning of bulk coaxial deformation in
587 zones with opposite shear-senses.
588
589 *6.4. Comparison with inclusion-trail data from NW-Iberia*
590
591 Figure 14 compares the inclusion-trail- and field data presented here from southern
592 Brittany with that of Aerden (2004) for the 'Basal Unit' of the allochthonous complexes of
593 NW-Iberia. This unit is composed of orthogneisses and high-pressure micaschists
594 retrogressed to greenschist facies and represents the subducted margin of Gondwana (Arenas
595 et al, 1995; Martínez-Catalán, 1996). Thus, it occupies a similar structural position as the
596 Pouldu Schists below an ophiolitic unit. Three sets of inclusion trails striking E-W, NE-SW
597 and NNW-SSE were distinguished in this unit preserved within plagioclase and garnet
598 porphyroblasts. The oldest of these has an E-W trend and can be linked to a high-pressure
599 event dated 370-360Ma (Santos Zalduegui, et al. 1995; Abati et al., 2010; Li & Massonne,
600 2017), hence synchronous with prograde metamorphism in Ile de Groix (Bosse et al., 2005).
601 The 2 younger internal foliations sets formed at lower pressures and their age is only loosely
602 constrained to pre-320 Ma. The paleogeographic reconstruction of Fig. 14a fits the northern
603 continental margin of Iberia to the conjugate margin of south Brittany involving 20°
604 clockwise back-rotation of Iberia. This produces a remarkably good match of inclusion-trail
605 orientations in both regions (Fig. 14b), yet raises a relative timing problem. Aerden (2004)
606 interpreted that NNW-SSE striking inclusion trails in the Basal Unit (marked blue in Fig. 14)
607 post-date E-W ones (yellow), opposite to what has been concluded in this paper for Ile de
608 Groix. Since Aerden's (2004) relative timing was based on only one sample (sample 1. - Fig.
609 14a), we believe there is scope for further testing this chronology via study of new samples

610 with the now available 3-D techniques. The timing of NE-SW striking inclusion trails in NW
611 Iberia (marked red in Fig. 14a) is based on more abundant microstructural and field criteria,
612 ruling out a correlation with the also NW-SE striking but much older inclusion-trail set in Ile
613 de Groix. A correlation is possible, though, with the internal foliations of the 2 samples from
614 the Central Armorican Domain, and the crenulation cleavages observed in some of the Pouldu
615 schist samples (Fig. 3c and d).
616 We checked the curvature sense of 'rotational' inclusion trails in 7 of Aerden's (2004)
617 samples associated with the subduction related E-W to NW-SE trending FIAs (marked yellow
618 in Fig. 14a). In samples 3, 4, 10, 14 and 20, inclusion trails curve anticlockwise viewing west;
619 in samples 2 and 19 they curve clockwise. The larger number of anticlockwise trails is the
620 same as observed in Ile de Groix, although we realize that this coincidence needs to be further
621 tested.
622
623 **7. Conclusion**
624
625 (1) Garnet and pseudomorphed lawsonite porphyroblasts in blueschist-eclogite facies
626 rocks of Ile de Groix preserve a succession of 3 sets of steeply dipping inclusion-trails
627 striking NW-SE, NNW-SSE and WNW-ESE. They can be interpreted to record 3 episodes of
628 differently oriented compression orthogonal to their strikes during subduction of oceanic crust
629 and prograde metamorphism dated 365-355Ma (Bosse et al. 2005).
630 (2) The consistency of inclusion-trail orientations across Groix island implies limited
631 porphyroblast rotation, and hence an origin of sigmoid- and spiral inclusion trails by
632 overgrowth of successive crenulation cleavages (e.g. Bell et al., 1986; Aerden, 1995; Stallard
633 & Hickey, 2001) rather than progressive shearing and porphyroblast rotation. This re-
634 interpretation reconciles a previous conflict between the dominant curvature sense of
635 inclusion trails on Ile de Groix with north- or north-westward directed subduction of
636 Gondwana under Armorica, as is indicated by the general tectono-metamorphic zonation of
637 the Ibero-Armorican Arc.
638 (3) Porphyroblast growth was followed by the development of a subhorizontal
639 crenulation cleavage accompanying retrogression and exhumation (Shelley & Bossière, 1999)
640 and dated 355-345Ma (Bosse et al., 2005). This foliation fully transposed earlier steeply
641 dipping fabrics preserved within porphyroblasts and produced inconsistent (opposite) shear-
642 sense criteria, such as asymmetric strain shadows, shear bands and quartz c-axes fabrics.
643 Together with cm- to decametre-scale fold-interference patterns this indicates vertical sub-

coaxial shortening, which we tentatively relate to gravitational spreading of a thrust nappe during continuous plate-convergence.

(4) Fold axes parallel stretching and variable fold geometries ranging from cylindrical to sheath-like did not result from progressive shearing parallel to a single foliation (cf. Cobbold & Quinquis, 1980) but from vertical shortening and horizontal shearing of pre-existing folds with subvertical axial-planes.

(5) Inclusion-trails studied in 4 greenschist samples from the Pouldu schists (part of the footwall of the Ile-de-Groix ophiolitic nappe) strike WNW-ESE, subparallel to the youngest set of inclusion-trails on Groix island. They record continued N-S compression in the Carboniferous possibly synchronous with gravitational spreading in the hangingwall, but in any case also afterwards when a late set of E-W trending chevron-style folds developed on Groix island.

(6) The 3 sets of inclusion trails documented in southern Brittany can be tentatively correlated with 3 similar sets in NW-Iberia (Aerden, 2004) with similar strikes, after the northern margin of Iberia is placed back against the conjugate margin of southern Brittany. This match suggests about 20° anticlockwise rotation of Iberia during opening of the Gulf of Biscay, somewhat less as commonly deduced from paleomagnetism (e.g. Gong et al., 2009).

Acknowledgements

The first author wishes to thank José Ramón Martínez Catalán for his guidance and friendship during a postdoc in Salamanca (1996-1999). We thank Michel Ballèvre for helping obtain permission from the Préfecture du Morbihan to collect samples on Ile de Groix and for suggesting we include the Pouldu schists in our study. Ile de Groix national-park guide Catherine Robert (and her dog) provided DA with helpful information and pleasant company during field work. We thank Fátima Linares-Ordoñez for X-ray scanning our samples, and Bernhardt Schulz for clarifying various aspects about the petrology of the study area. The authors are very grateful to 2 anonymous reviewers who provided constructive comments, and the handling editors of Solid Earth. The research was made possible by a travel grant from the Junta de Andalucía to DA in 2006, Spanish-government project CGL2016-80687-R AEI/FEDER, project RNM148 of the Andalusia Autonomous government.

678 **References**

679

680 Abu Sharib, A.S.A.A., Bell T.H. (2011) Radical changes in bulk shortening directions during
681 orogenesis: Significance for progressive development of regional folds and thrusts.
682 Precambrian Research 188, 1–20.
683 Abu Sharib, A.S.A.A., and Sanislav, I.V. (2013) Polymetamorphism accompanied switching
684 in horizontal shortening during Isan Orogeny: example from the Eastern Fold Belt, Mount
685 Isa Inlier, Australia. Tectonophysics, 587. pp. 146-167.
686 Aerden, D. G. A. M. (1994). Kinematics of orogenic collapse in the Variscan Pyrenees
687 deduced from microstructures in porphyroblastic rocks from the Lys-Caillaouas massif.
688 Tectonophysics, 238(1–4). https://doi.org/10.1016/0040-1951(94)90053-1
689 Aerden, D.G.A.M. (1995) Porphyroblast non-rotation during crustal extension in the Variscan
690 Pyrenees. Journal of Structural Geology 17, 709-726.
691 Aerden, D.G.A.M. (1998) Tectonic evolution of the Montagne Noire and a possible orogenic
692 model for syn-collisional exhumation of deep rocks, Hercynian belt, France. Tectonics 17,
693 62-79.
694 Aerden, D.G.A.M. (2004) Correlating deformations in the Iberian Massif (Variscan belt)
695 using porphyroblasts; implications for the development of the Ibero-Armorican Arc.
696 Journal of Structural Geology 26, 177-196.
697 Aerden, D.G.A.M., Bell, T.H., Puga, E., Sayab, M., Lozano, J.A., Díaz de Federico, A.
698 (2013) Multi-stage mountain building vs. Relative plate motions in the Betic Cordillera
699 deduced from integrated microstructural and petrological analysis of porphyroblast
700 inclusion trails. Tectonophysics 587, 188-206.
701 Aerden, D.G.A.M., Malavieille, J. (1999) Origin of a large-scale fold nappe in the Montagne
702 Noire,Variscan belt, France. Journal of Structural Geology 21, 1321-1333
703 Aerden, D. G. A. M., & Sayab, M. (2017). Probing the prodigious strain fringes from Lourdes.
704 Journal of Structural Geology, 105. https://doi.org/10.1016/j.jsg.2017.11.001
705 Aerden, D.G.A.M., Ruiz-Fuentes, A. (2020) X-ray computed microtomography of spiral
706 garnets: A new test of how they form. Journal of Structural Geology 136.
707 https://doi.org/10.1016/j.jsg.2020.104054
708 Ali, A. (2010). The tectono-metamorphic evolution of the Balcooma Metamorphic Group,
709 north-eastern Australia: a multidisciplinary approach. Journal of Metamorphic Geology,
710 28(4), 397–422. https://doi.org/10.1111/j.1525-1314.2010.00871.x

711 Arenas, R., Rubio Pascual, F., Díaz García, F., Martínez Catalán, J.R. (1995) High-pressure
712 micro-inclusions and development of an inverted metamorphic gradient in the Santiago
713 Schists (Ordenes Complex, NW Iberian Massif, Spain): evidence of subduction and
714 syncollisional decompression. Journal of Metamorphic Geology 13, 141–164.
715 Arenas, R., Sanchez Martinez, S., Diez Fernandez, R., Gerdes, A., Abati, J., Fernandez-
716 Suarez, J., Andonaegui, P., Cuadra, P.G., Carmona, A.L., Albert, R., Fuenlabrada, J.M.,
717 Rubio Pascual, F.J. (2016) Allochthonous terrains involved in the Variscan suture of NW
718 Iberia: A review of their origin and tectonothermal evolution Earth-Science Reviews 161,
719 140-178.
720 Audren C., Triboulet C. (1993). Les chemins pression-température enregistrés au cours de la
721 formation de plis non-cylindriques dans les schistes bleus de l'Ile de Groix (Bretagne
722 méridionale, France). Comptes Rendus de l'Académie des Sciences de Paris, (II) 317, 259-
723 265.
724 Audren, C., Triboulet, C., Chauris, L., Lefort, J. P., Vigneresse, J. L., Audrain, J.,
725 Thiéblemont, D., Goyallon, J., Jégouzo, P., Guennoc, P., Augris, C. & Carn, A. (1993).
726 Notice explicative de la feuille Ile de Groix à 1/25 000 (carte géologique). Orléans: BRGM.
727 Azor, A., Rubatto, D., Simancas, J.F., González Lodeiro, F., Martínez Poyatos, D.,
728 MartínParra, L.M., Matas, J., (2008) Rheic Ocean ophiolitic remnants in southern Iberia
729 questioned by SHRIMP U–Pb zircon ages on the Beja-Acebuches amphibolites. Tectonics
730 27, TC5006.
731 Ballevre, M; Pitra, P; Bohn, M., (2003) Lawsonite growth in the epidote blueschists from the
732 Ile de Groix (Armorican Massif, France): a potential geobarometer. Journal of
733 Metamorphic Geology 21, 723-735.
734 Ballèvre, M., Bosse V., Ducassou, C., Pitra. P., (2009) Palaeozoic history of the Armorican
735 Massif: Models for the tectonic evolution of the suture zones. C. R. Geoscience 341 (2009)
736 174–201.
737 Ballevre, M., Bosse, V., Dabard, M.P., Ducassou, C., Fourcade, S. et al., (2015) Histoire
738 Géeologique du massif Armoricain : Actualitée de la recherche. Bulletin de la Sociétée
739 Géologique et Minéralogique de Bretagne, Société géologique et minéralogique de
740 Bretagne, (2013, (D), 10-11, pp.5-96. <insu-00873116>
741 Béchennec, F., Hallégouët, B., Thiéblemont, D., Thinon, I. (2012). Notice explicative, Carte
742 géol. France (1/50 000), feuille Lorient (383). Orléans : BRGM, 206 p.
743 Bell, T.H., (1985) Deformation partitioning and porphyroblast rotation in metamorphic rocks:
744 A radical reinterpretation. Journal of Metamorphic Geology 3, 109-118.

745 Bell T.H., Bruce M.D. (2006). The internal inclusion trail geometries preserved within a first
746 phase of porphyroblast growth. Journal of Structural Geology 28, 236-252.
747 Bell, T.H., Fay, C. (2016) Holistic microstructural techniques reveal synchronous and
748 alternating andalusite and staurolite growth during three tectonic events resulted from
749 shifting partitioning of growth vs deformation. Lithos 262, 699–712.
750 Bell, T.H., Forde, A., Wang, J., (1995) A new indicator of movement direction during
751 orogenesis - measurement technique and application to the Alps. Terra Nova 7, 500-508.
752 Bell, T.H., Hickey, K.A., Upton, G.J.G., (1998) Distinguishing and correlating multiple
753 phases of metamorphism accross a multiply deformed region using the axes of spiral,
754 staircase, and sigmoidally curved inclusion trails in garnet. Journal of Metamorphic
755 Geology 16, 767-794.
756 Bell, T.H., Johnson, S.E., 1989. Porphyroblast inclusion trails: the key to orogenesis. Journal
757 of Metamorphic Geology 7, 279-310.
758 Bell, T.H., Johnson, S.E., Davis, B., Forde, A., Hayward, N., Wilkins, C., (1992)
759 Porphyroblast inclusion-trail orientation data: eppure non son girate! Journal of
760 Metamorphic Geology 10, 295-307.
761 Bell. T. H., Rubenach, M. J. & Flemming, P. D., (1986) Porphyroblast nucleation, growth and
762 dissolution in regional metamorphic rocks as a function of deformation partitioning during
763 foliation development. Journal of Metamorphic Geology, 4, 37–67.
764 Bell, T.H, Sapkota, J., (2012) Episodic gravitational collapse and migration of the mountain
765 chain during orogenic roll-on in the Himalayas. Journal of Metamorphic Geology 30, 651-
766 666.
767 Bell, T.H., Welch, P.W., 2002. Prolonged Acadian Orogenesis: revelations from foliation
768 intersection axis (FIA) controlled monazite dating of foliations in porphyroblasts and
769 matrix. American Journal of Science, 302, 549–581.
770 Bosse V., Ballèvre M., Vidal O., (2002) Ductile thrusting recorded by the garnet isograd from
771 blueschist-facies metapelites of the Île de Groix, Armorican Massif, France. Journal of
772 Petrology 43, 485-510.
773 Bosse, V., Féraud, G., Ballèvrec, M., Peucatc, J.J., Corsini, M., (2005) Rb–Sr and 40Ar/39Ar
774 ages in blueschists from the Ile de Groix (Armorican Massif, France): Implications for
775 closure mechanisms in isotopic systems. Chemical Geology 220 (2005) 21– 45.
776 Boudier, F., Nicolas, A. (1976) Interprétation nouvelle des relations entre tectonique et
777 métamorphisme dans l'île de Groix (Bretagne). Bull. Soc. Géol. France, S7-XVIII (1),
778 135–144.

779 Bucher, .H., 1956. Role of gravity in orogenesis. Bull. Geol. Soc. Am. 67, 1295-1318.
780 Cannat, M., (1985) Quartz microstructures and fabrics in the island of Groix (Brittany,
781 France). Journal of Structural Geology 7, 555–562.
782 Cobbold, P.R., Quinquis, H., (1980) Development of sheath folds in shear regimes. Journal of
783 Structural Geology 2, 119-126.
784 Cogné J., Daniel, J., Ruhland, M., (1966) L'Ile de Groix. Etude structurale d'une série
785 métamorphique à glaucophane en Bretagne méridionale. In: Bulletin du Service de la carte
786 géologique d'Alsace et de Lorraine, 19-1, pp. 41-96. doi :
787 https://doi.org/10.3406/sgeol.1966.1298
788 Díaz García, F., Arenas, R., Martínez Catalán, J.R., González del Tánago, J., and Dunning,
789 G.R., (1999) Tectonic evolution of the Careón ophiolite (northwest Spain): A remnant of
790 the oceanic lithosphere in the Variscan Belt. Journal of Geology, v. 107, p. 587–605.
791 Doube M, Kłosowski MM, Arganda-Carreras I, Cordeliéres F, Dougherty RP, Jackson J,
792 Schmid B, Hutchinson JR, Shefelbine SJ. (2010) BoneJ: free and extensible bone image
793 analysis in ImageJ. Bone 47:1076-9. doi: 10.1016/j.bone.2010.08.023
794 Engels, J.P. (1972). The catazonal polymetamorphic rocks of Cabo Ortegal(NW Spain), a
795 structural and petrofabric study. Leidse Geologische Mededelingen 48, 83–133
796 Faure, M., Bé Mézème, E., Cocherie, A., Rossi, P., Chemenda, A., Boutelier, D., (2008)
797 Devonian geodynamic evolution of the Variscan Belt, insights from the French Massif
798 Central and Massif Armoricain, Tectonics, 27, TC2005, doi:10.1029/2007TC002115.
799 Fay, C., Bell, T.H., Hobbs, B.E., 2008. Porphyroblast rotation versus nonrotation: Conflict
800 resolution! Geology 36, 307-310.
801 Felix, C., Fransolet, A.M., (1972) Pseudomorphes á épidote s.l., paragonite, muscovite s.l.,
802 chlorite, albite. de porphyroblastes de lawsonite (?) dans les glaucophanites de l'Île de
803 groix (bretagne – France). Annales de la Société Geologique de Belgique 95, 323–334.
804 Gong, Z., Langereis, C.G., Mullender, T.A.T. , (2008) The rotation of Iberia during the
805 Aptian and the opening of the Bay of Biscay. Earth and Planetary Science Letters 273, 80–
806 93.
807 Hayward, N., (1990) Determination of early fold axis orientations in multiply deformed rocks
808 using porphyroblast inclusion trails. Tectonophysics 179, 353-369.
809 Hayward, N., (1992) Microstructural analysis of the classical spiral garnet porphyroblasts of
810 south-east Vermont: evidence for non-rotation. Journal of Metamorphic Geology 10, 567-
811 587.

812 Huddlestone-Holmes, C.R., Ketcham, R.A., (2010) An X-ray computed tomography study of
813 inclusion trail orientations in multiple porphyroblasts from a single sample.
814 Tectonophysics 480, 305–320.
815 Kim, H. S., & Ree, J.-H. (2013). Permo-Triassic changes in bulk crustal shortening direction
816 during deformation and metamorphism of the Taebaeksan Basin, South Korea using
817 foliation intersection/inflection axes: Implications for tectonic movement at the eastern
818 margin of Eurasia during the Songrim (Indosinian) orogeny. Tectonophysics, 587(SI),
819 133–145. https://doi.org/10.1016/j.tecto.2012.08.033
820 Lagarde, J.L. (1980). La déformation des roches dans les domaines àschistosité
821 subhorizontale. Applications à la nappe du Canigou-Roc de France (Pyrénées orientales) et
822 au complexe crystallophyllien de Champtoceaux (Massif armoricain). Unpublsihed PhD
823 thesis, Université de Rennes, 170 p.
824 Li, B., Massonne, H.J., (2017) Contrasting metamorphic evolution of metapelites from the
825 Malpica-Tuy unit and the underlying so-called parautochthon at the coast of NW Spain.
826 Lithos 286–287, 92–108. http://dx.doi.org/10.1016/j.lithos.2017.06.003
827 Mares, V.M., (1998) Structural development of the Soldiers Cap Group in the Eastern Fold
828 Belt of the Mt Isa Inlier: a successive of horizontal and vertical deformation events and
829 large-scale shearing. Aust. J. Earth Sci. 45, 373–387.
830 Martínez Catalaín, J.R., Arenas, R., Díaz García, F., Rubio Pascual, F.J., Abati, J., Marquínez,
831 J., (1996) Variscan exhumation of a subducted Palaeozoic continental margin: the basal
832 units of the Ordenes Complex, Galicia, NW Spain. Tectonics 15, 106–121.
833 Martínez Catalán J.R., Arenas, R., Díaz García, F., Abati, J. 1997. Variscan accretionary
834 complex of northwest Iberia: Terrane correlation and succession of tectonothermal events.
835 Geology 25, p. 1103–1106.
836 Martínez Catalán J.R. (2011). Are the oroclines of the Variscan belt related to late Variscan
837 strike-slip tectonics? Terra Nova 23, 241–247. doi: 10.1111/j.1365-3121.2011.01005.x
838 Matte, P., (2001) The Variscan collage and orogeny (480-290 Ma) and the tectonic definition
839 of the Armorica microplate: a review. Terra Nova 13, 122-128.
840 Merle, O., The building of the central Swiss Alps: An experimental approach. Tectonophysics,
841 165, 41-56, 1989.
842 Munro, M. A., & Blenkinsop, T. G. (2012). MARD - A moving average rose diagram
843 application for the geosciences. Computers & Geosciences, 49, 112–120.
844 https://doi.org/10.1016/j.cageo.2012.07.012

845 Philippon M., Brun J.-P. et Gueydan F., (2009) Kinematic records of subduction and
846 exhumation in the Île de Groix blueschists (Hercynian belt ; Western France). Journal of
847 Structural Geology 31, 1308-1321.
848 Quinquis, H., Audren, C., Brun, J. P. & Cobbold, P. R. (1978) Intense shear in Ile de Groix
849 blueschists and compatibility with subduction or obduction. Nature, Lond. 273, 43-45.
850 Quinquis, H., (1980) Schistes bleus et déformation progressive: l'exemple de l'Île de Groix
851 (Massif Armoricain). Université de Rennes 1.
852 Quinquis, H., Choukroune, P., (1981) The Ile de Groix blueschists in the Hercynian chain -
853 kinematical implications. Bulletin de la societe geologique de France 2, 409-418.
854 Rosenfeld, J.L., (1970) Rotated garnets in metamorphic rocks. Geological Society of America
855 Special Paper 129, 102pp.
856 Sayab, M., (2005) Microstructural evidence for N–S shortening in the Mount Isa Inlier (NW
857 Queensland, Australia): the preservation of early W–E-trending foliations in
858 porphyroblasts revealed by independent 3D measurement techniques. Journal of Structural
859 Geology 27, 1445-1468.
860 Sayab, M., Aerden, D., Kuva, J., Hassan, W.U., 2021. Tectonic evolution of the Karakoram
861 metamorphic complex (NW Himalayas) reflected in the 3D structures of spiral garnets:
862 Insights from X-ray computed micro-tomography. Geoscience Frontiers 3. DOI:
863 https://doi.org/10.1016/j.gsf.2020.11.010
864 Shah, S.Z. Sayab, M., Aerden, D.G.A.M, Asif-Kahn, M. (2011) Foliation intersection axes
865 preserved in garnet porphyroblasts from the Swat area, NW Himalaya: A record of
866 successive crustal shortening directions between the Indian plate and Kohistan-Ladakh
867 Island Arc. Tectonophysics 509, 14-32.
868 Shelley, D., Bossieère, G., (1999) Ile de groix: retrogression and structural developments in
869 an extensional régime. Journal of Structural Geology 21, 1441–1455.
870 Schindelin, J., Arganda-Carreras, I., Frise, E., Kaynig, V., Longair, M., Pietzsch, T., Preibisch,
871 S., Rueden, C., Saalfeld, S., Schmid, B., Tinevez, J.Y., White, D.J., Hartenstein, V.,
872 Eliceiri, K., Tomancak, P., Cardona, A., (2012) Fiji: an open-source platform for
873 biological-image analysis. Nature Methods 9, 676-682.
874 Schulz, B., Audren, C., Triboulet, C. (1998) Regional vs contact metamorphism of garnet
875 metapelites in the vicinity of Late Variscan granites (Central Armorican Domain, Brittany,
876 France). Geologische Rundschau 87, 78-93.

Schulz, B., Triboulet., C., Audren., C; Pfeifer., H.R., Gilg, A., (2001) Two-stage prograde and retrograde Variscan metamorphism of glaucophane-eclogites, blueschists and greenschists from Ile de Groix (Brittany, France) International Journal of Earth Sciences, 90, 871-889.

Spry, A., 1633) The origin and sigdicance of snowball structure in garnet. Journal of Petrology 4, 211-222.

Stallard, A., Hickey, K., 2001. Shear zone vs folding origin for spiral inclusion trails in the Canton Schist. Journal of Structural Geology 23, 1845-1864.

Stallard, A.R., Hickey, K.A., Upton, G.J., (2003) Measurement and correlation of microstructures: the case of foliation intersection axes. Journal of Metamorphic Geology 21, 241–252.

Triboulet, C., (1974) Les glaucophanites et roches associe´es de l'île de Groix (Morbihan, France): étude minéralogique et pétrogénétique. Contributions to Mineralogy and Petrology, 45, 65–90.

Triboulet, C. (1992) Subglaucophanic greenschists from Le-Pouldu, a transitional area between blueschists and amphibolites from a paleozoic single metamorphic belt in south Brittany, France. Comptes Rendus de l'Academie des Sciences serie II: 315, 697-703

Van Zuuren, A., 1969. Structural petrology of an area near Santiago de Compostella (NW Spain). Leidse Geologische Mededelingen 45, 1–71.

Zhang Q., Fossen, H., 2020. The dilemma of asymmetric porphyroclast systems and sense of shear. Journal of Structural Geology 130. https://doi.org/10.1016/j.jsg.2019.103893

Zwart, H., (1962) On the determination of polymorphic mineral associations and its application to the Bosost area (central Pyrenees). Geologisches Rundschau, 52, 38-65.

FIGURE CAPTION

Fig. 1. (a) Traditional rotational interpretation of sigmoidal and spiral-shaped inclusion trails and the range (purple) of inclusion-trail strikes predicted by this model in rocks from Ile de Groix. (b) 'Non-rotational' interpretation of inclusion trails formed by overgrowth of successive crenulation cleavages and the predicted range of inclusion-trail strikes for Ile de Groix. (c) Actually measured inclusion-trail strikes in 10 samples from Ile de Groix. Note that they better match the predictions of the non-rotation model.

910 Fig. 2. (a) Simplified geological maps of southern Brittany and NW-Iberia showing the
911 location of ophiolite outcrops and samples studied herein and by Aerden (2004) in NW Iberia.
912 (b) Schematic N-S cross-section through after Ballèvre et al. (2015) showing the structural
913 relationships between tectonic units in the Variscan orogen.
914
915 Fig. 3. (a) Stretching lineation pattern in Ile de Groix and sample locations. (b) Moving-
916 average rose diagrams for inclusion-trail strikes. Pie-cake symbols in circles give the average
917 trend and plunge direction of FIAs in samples as determined from radial sets of thin sections.
918 Small spirals inside these pie cakes indicate the curvature sense of inclusion-trails as seen
919 when viewing down FIA plunge (anticlockwise in G14, G12, G11; clockwise in G19 and G7).
920 Pink, blue, yellow and red trend lines code for 4 different inclusion trail sets distinguished in
921 this paper from older to younger. (c) Inclusion-trail strikes in Pouldu-schists samples and
922 Tréogat formation (AU1). Arrows represent fold axes measured in outcrop. (d) Data from 2
923 staurolite-kyanite schists of the Central Armorican Domain.
924
925 Fig. 4. (a, b) Line drawings of inclusion trails and associated truncations (yellow lines) in
926 differently striking vertical thin sections of G7 and G14. Half arrows indicate the strike of
927 each section and way up. (c) Binned rose diagram plotting the angles of all dashes
928 representing inclusion-trails in (a) and (b) as measured with the 'Analyse Particle' tool of Fiji.
929 The broadly bimodal distribution reflects the presence of 2 or more sets of inclusion-trail
930 planes, consistent with overgrowth of successive crenulation cleavages rather than with
931 continuous rotation of syntectonic porphyroblasts.
932
933 Fig. 5. (a) Microstructural line drawings traced on photographs of thin sections of greenschist
934 samples PO2 and PO3 containing albite porphyroblasts. Three foliations can be recognized.
935 S2 corresponds to the macroscopic cleavage and crenulates an older S1. S3 corresponds to
936 weak subhorizontal crenulations. (b) Interpretation of porphyroblast growth history. Most
937 albite porphyroblasts form early during D2 when they overgrow S1. Further grow early
938 during D3 produces additional inclusion trails of S2.
939
940 Fig. 6. Photographs of G11. (a and b) Garnet porphyroblast (parallel and crossed polars) with
941 sigmoidal trails in a N-S striking vertical section. Barb of N-arrow points upward. Note top-
942 to-the south shear sense suggested by asymmetric strain shadows consistent with a non-
943 rotational interpretation of the inclusion trails. (c) Garnet with spiral-shaped inclusion trails

944 with a truncation surface between the porphyroblast core and rim. (d) Opaque mineral with
945 elongate shape replaced by goethite. (e and f). Lawsonite pseudomorphs (parallel and crossed
946 polars) showing weakly sigmoidal inclusion trails oriented oblique to the matrix foliation. (g)
947 Tomographic image of spiral inclusion trails garnet in G12. (h) Tomographic image of an
948 elongate lawsonite pseudomorph, a garnet porphyroblast (Gt) and an opaque mineral.
949
950 Fig. 7. Stereoplots (equal angle, lower hemisphere; made with the program 'Stereonet') for
951 internal foliations and FIAs preserved within garnet crystals and lawsonite pseudomorphs in
952 samples G11 and G12, as well as long- and short axes of best-fit ellipsoids calculated for
953 opaques minerals present in the matrix of both samples (contoured using a blue ramp). See
954 legend and main text for detailed description of this data. The stereoplot data can be colour
955 matched to representative oriented maps (note North arrow) of inclusion trails shown at the
956 bottom of the Figure, traced on high-resolution photographs of horizontal thin sections. A
957 lawsonite pseudomorph (Laws.) is also drawn.
958
959 Fig. 8. Tomographic images and microstructural data for sample G14. (a) Stereoplot for
960 internal foliation planes, FIAs (grey boxes), long- and short axes of opaque minerals, and
961 axial plane of cm-scale fold. (b and c) Map- and cross-section views of a fold outlined by an
962 epidote-rich layer. Its axial trace trends NNE-SSW and is transected by N-S trending cleavage
963 zones also visible in (d). Tomographic cross-section showing refolding with subhorizontal
964 axial planes of the fold in (b) implying a component of vertical flattening.
965
966 Fig. 9. (a) 3D microstructural data for sample G3. See legend and section 4.5. for detailed
967 description of this data. (b) Field data collected by Claude Audren near sample G7 at Plage du
968 Trech and the average FIA trend (pink pie-cake) we determined for this sample from radial
969 thin sections. The FIA trend is parallel to fold axes measurements. Note that this conflicts
970 with progressive shearing, fold-limb rotation and porphyroblast rotation. Stretching lineations
971 vary significantly reflecting polyphase deformation. (c) Microstructural data for G20. See
972 legend and text of section 4.5 for detailed description.
973
974 Fig. 10. (a) Main foliation- and lineation- data from Cogné et al. (1966) re-plotted in equal-
975 area, lower hemisphere stereoplots for higher-grade eastern Groix and lower-grade western
976 Groix. The high-grade domain has a gently E to S dipping foliation. The lower-grade area has
977 moderately to steeply SW- and NE dipping foliations. The original plot files are included in

978 the electronic supplement. (b) Proposed interpretation of the structural relationship between
979 both domains separated by a thrust cutting pre-existing folds. (c) Re-drafted field sketch of
980 Boudier & Nicolas (1976; their Fig. 2) of an outcrop at Vallon du Lavoir showing upright
981 folds overprinted y a subhorizontal crenulation cleavage and associated refolding. (d) Re-
982 drafted field sketch of Cogné et al. (1966; their Fig. 5) at Vallon du Lavoir, which we
983 interpret as a tight anticline overprinted by a horizontal cleavage, in turn overprinted by a SW
984 dipping crenulation cleavage. The dashed line has been added .
985
986 Fig. 11. (a) Accurately re-drawn sketch by Claude Audren (1974; unpublished as far as we
987 know) of isoclinal folds at Vallon de Kérigant and corresponding structural data. Refolding of
988 a N165 trending lineation around the nose of a N120 trending fold is indicated. (b) Lineations
989 (L1) measured at nearby location Vallon du Lavoir by Boudier & Nicolas (1976) showing a
990 N120 trend maximum of L1 (yellow trend lines) oblique to B2 fold axes (blue trend lines). (c)
991 Structural data from the same authors collected across the island. Note the bimodal pattern of
992 L1 reflecting the strikes of the 3 sets of inclusion trails distinguished in Figs. 3, 6, 8 and 9.
993
994 Fig. 12. Conceptual models showing how vertical shortening and horizontal stretching can
995 have produce highly variable fold geometries depending on the original orientations of pre-
996 existing folds. Note how strongly curved fold axes can form without need of extremely large
997 shears trains. Adding a (horizontal) shearing component in the direction of X and/or Y can be
998 expected to have further modified the fold-interference patterns.
999
1000 Fig. 13. Asymmetric strain shadows and shear bands indicating mainly top-to-the north but
1001 some top-to-the south shearing as well in a N-S striking vertical section of G11. These criteria
1002 are associated with a horizontal transposition cleavage that post-dates garnet porphyroblasts.
1003 Note anticlockwise curvature sense of inclusion trails. The FIAs of these garnets plunge 45°
1004 west (see Fig. 7) highly oblique to the (horizontal) matrix foliation.
1005
1006 Fig. 14. (a) Inclusion trails-strikes measures for the present study and those of Aerden (2004)
1007 for 18 samples of the 'Basal Unit' of the allochthonous complexes of NW-Iberia. The
1008 microstructures are correlated as 4 sets marked pink, blue, yellow and red from the older to
1009 younger. Field data from Boudier and Nicolas (1976), Engels (1972) and van Zuuren (1969)
1010 correlated with the inclusion trails also show a good match. (b) Rose diagrams plotting all
1011 blue and yellow inclusion-trail trend lines in (a) for different amounts of Iberia back-rotation.

1012 The best-fit is obtained for 20° back-rotation, which coincides with the current angle between
1013 the North-Iberian and south-Brittany conjugate margins.

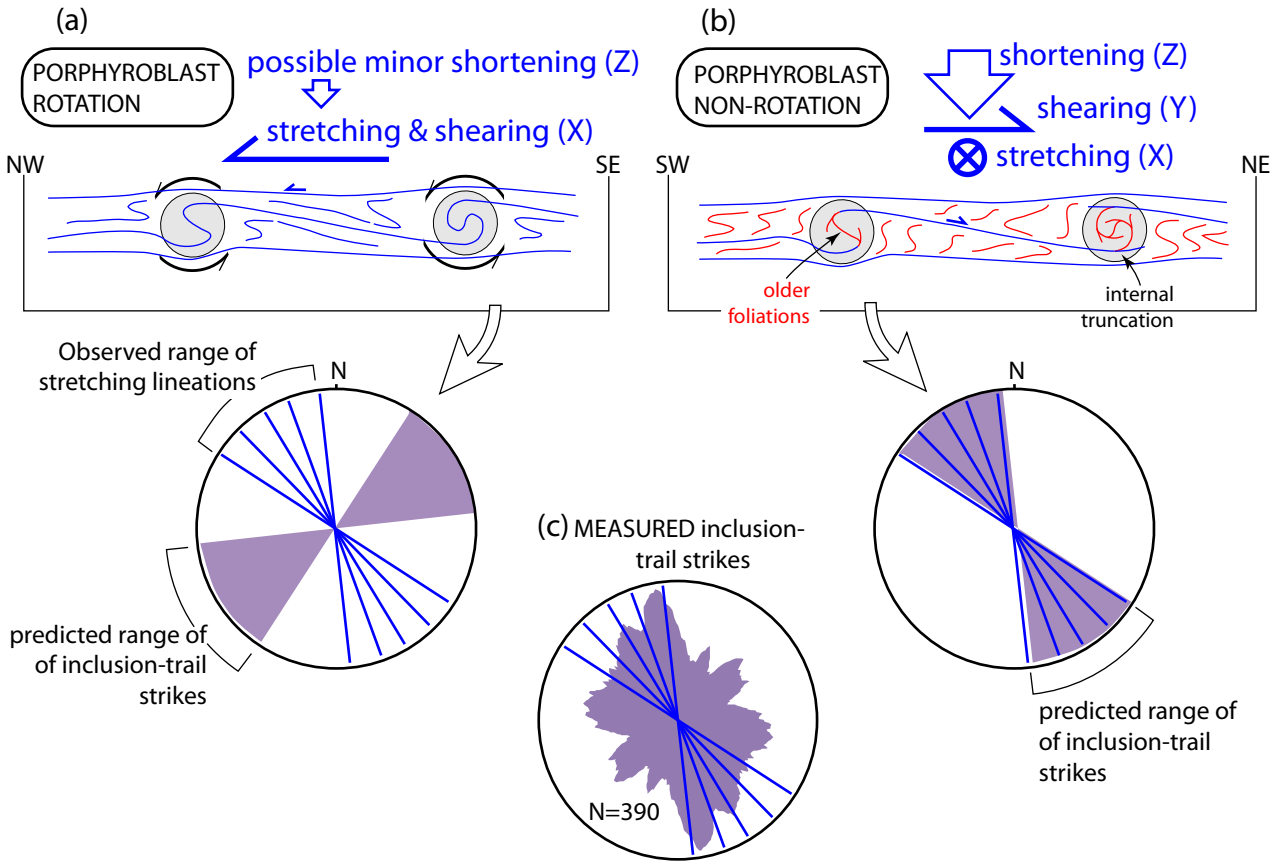
(a)
PORPHYROBLAST ROTATION
possible minor shortening (Z)
stretching & shearing (X)
NW
SE
Observed range of stretching lineations
N
predicted range of of inclusion-trail strikes
(b)
PORPHYROBLAST NON-ROTATION
shortening (Z)
shearing (Y)
stretching (X)
SW
NE
older foliations
internal truncation
N
predicted range of of inclusion-trail strikes
(c) MEASURED inclusion-trail strikes
N=390

FIG. 1

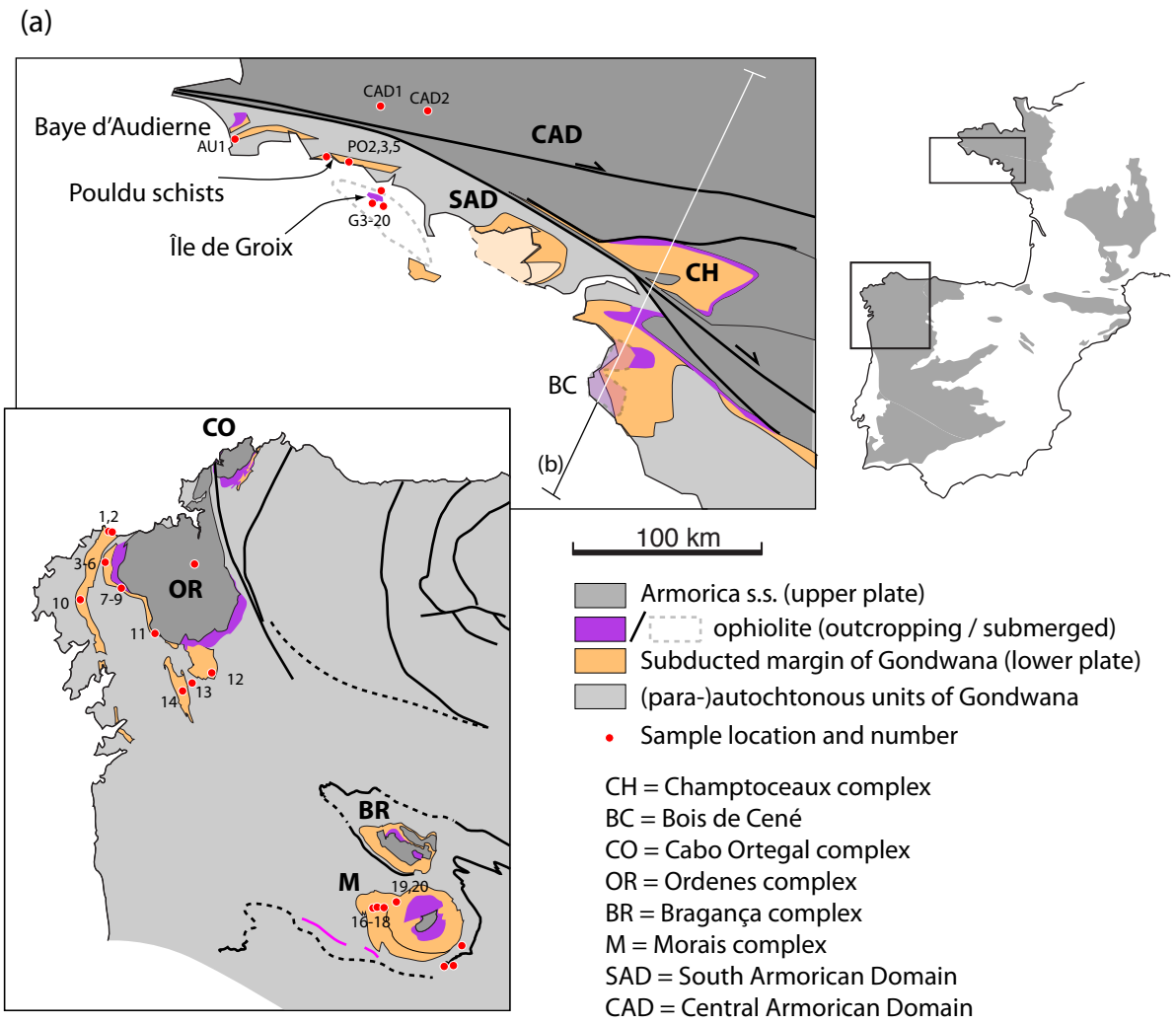
(a)
CAD1
CAD2
Baye d'Audierne
AU1
PO2,3,5
CAD
Pouldu schists
SAD
G3-20
Île de Groix
CH
BC
(b)
CO
1,2
3-6
OR
7-9
10
11
12
13
14
BR
M
19,20
16-18
100 km
Armorica s.s. (upper plate)
ophiolite (outcropping / submerged)
Subducted margin of Gondwana (lower plate)
(para-)autochtonous units of Gondwana
Sample location and number
CH = Champtoceaux complex
BC = Bois de Cené
CO = Cabo Ortegal complex
OR = Ordenes complex
BR = Bragança complex
M = Morais complex
SAD = South Armorican Domain
CAD = Central Armorican Domain

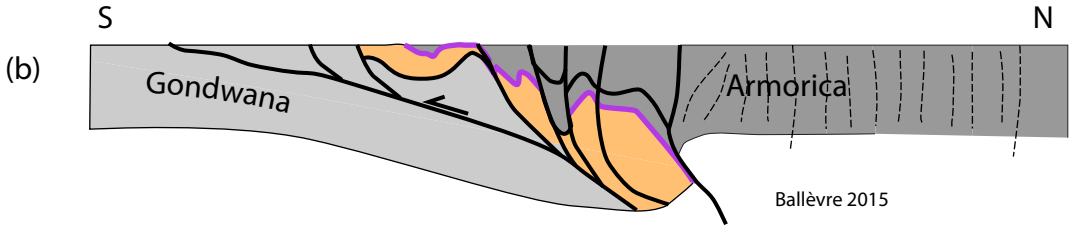
(b)
S
N
Gondwana
Armorica
Ballèvre 2015

FIG. 2

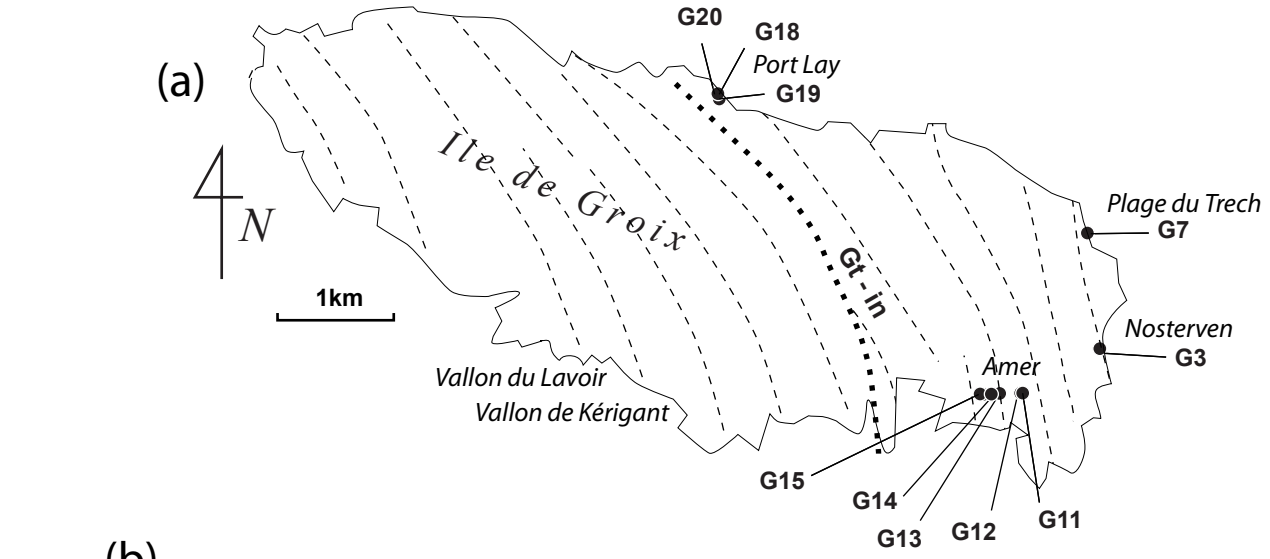
(a)
N
1km
Ile de Groix
Gt - in
G20
G18
Port Lay
G19
Plage du Trech
G7
Nosterven
G3
Amer
Vallon du Lavoir
Vallon de Kérigant
G15
G14
G13
G12
G11

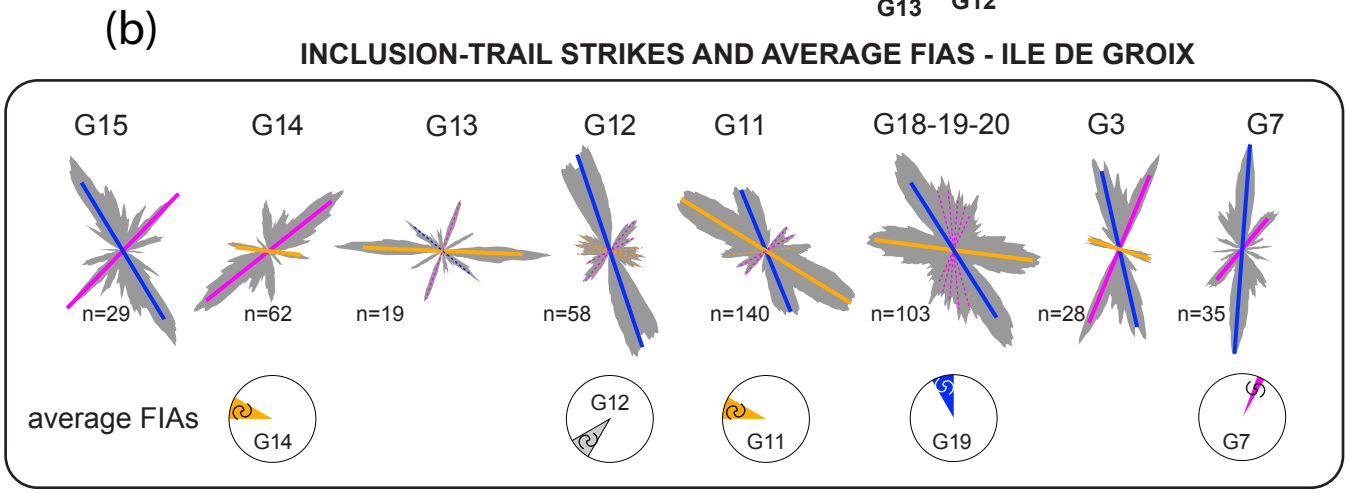
(b)
INCLUSION-TRAIL STRIKES AND AVERAGE FIAS - ILE DE GROIX
G15
G14
G13
G12
G11
G18-19-20
G3
G7
n=29
n=62
n=19
n=58
n=140
n=103
n=28
n=35
average FIAs
G14
G12
G11
G19
G7

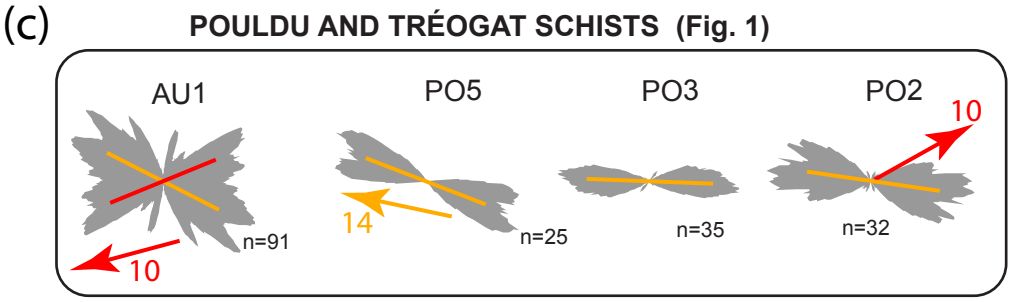
(c)
POULDU AND TRÉOGAT SCHISTS (Fig. 1)
AU1
PO5
PO3
PO2
n=91
10
14
n=25
n=35
10
n=32

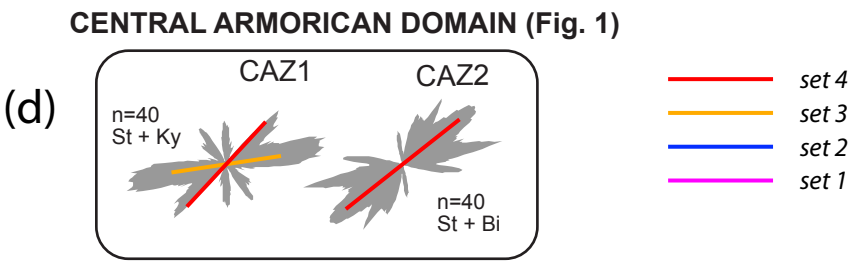
CENTRAL ARMORICAN DOMAIN (Fig. 1)
(d)
CAZ1
CAZ2
n=40
St + Ky
n=40
St + Bi
set 4
set 3
set 2
set 1

FIG. 3

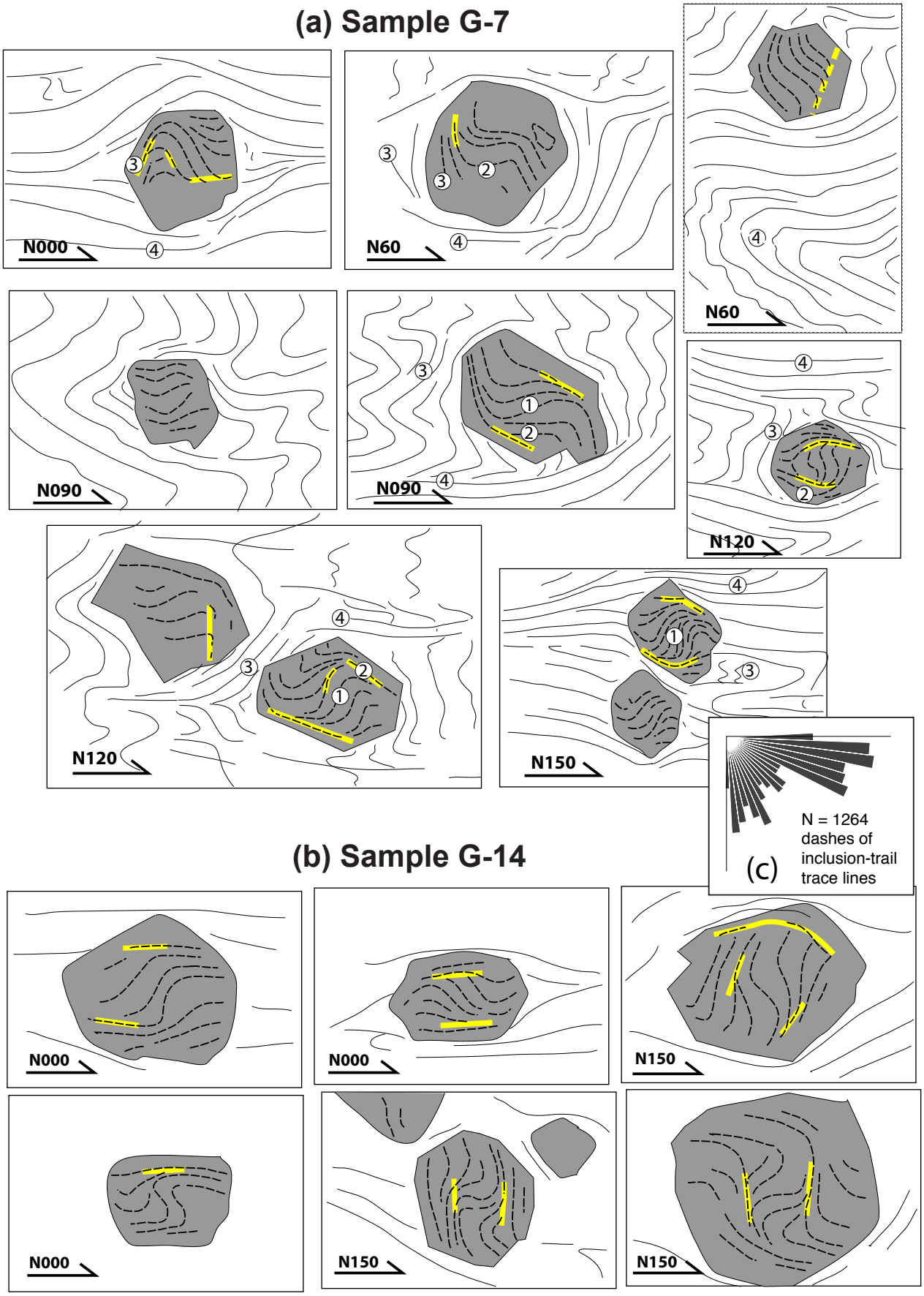
(a) Sample G-7
N000
N60
N60
N090
N090
N120
N120
N150
N = 1264
dashes of
inclusion-trail
trace lines
(c)
(b) Sample G-14
N000
N000
N150
N000
N150
N150

FIG. 4

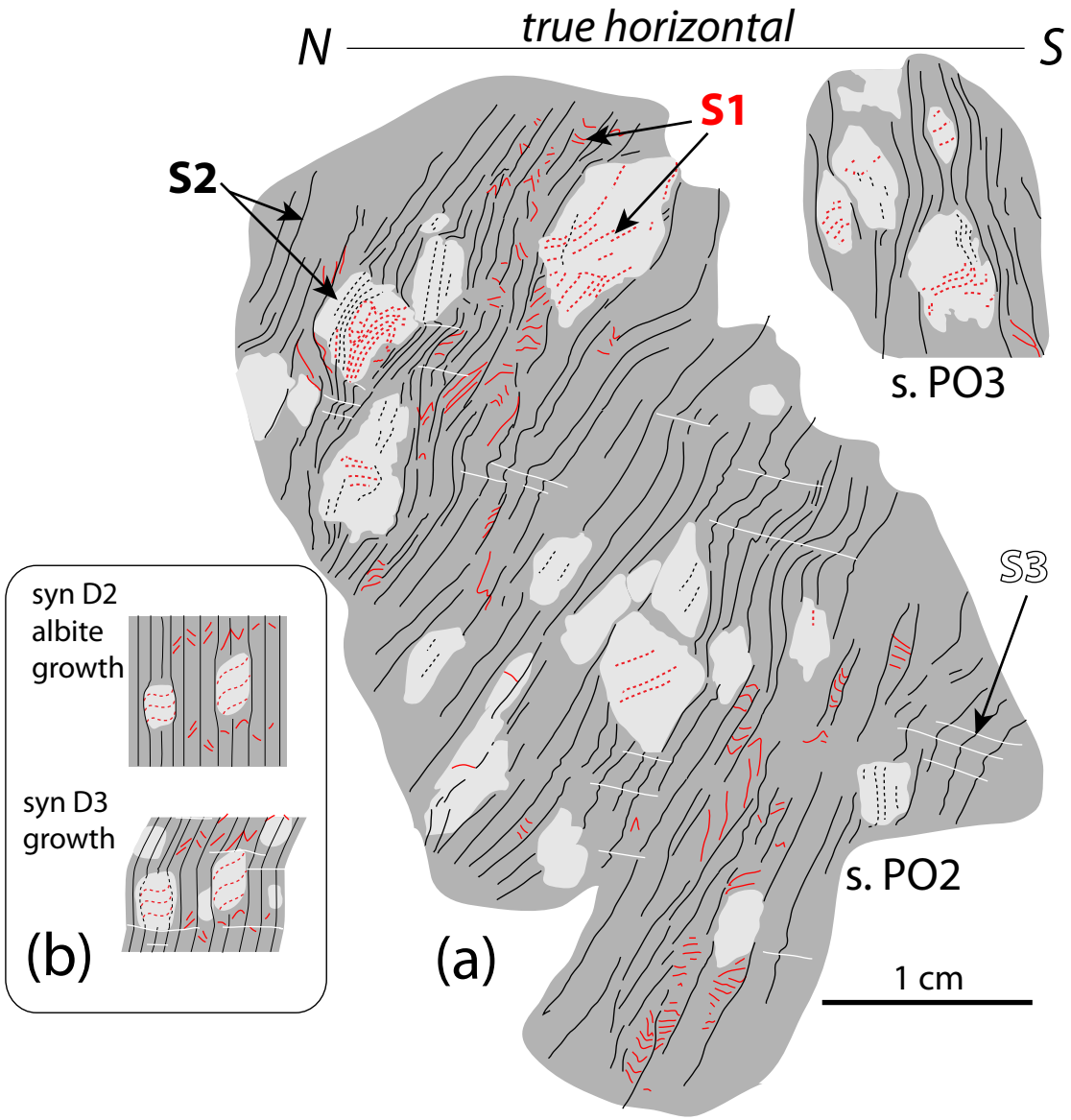
N
true horizontal
S
S1
S2
s. PO3
S3
s. PO2
1 cm
(a)
syn D2
albite
growth
syn D3
growth
(b)

Fig. 5

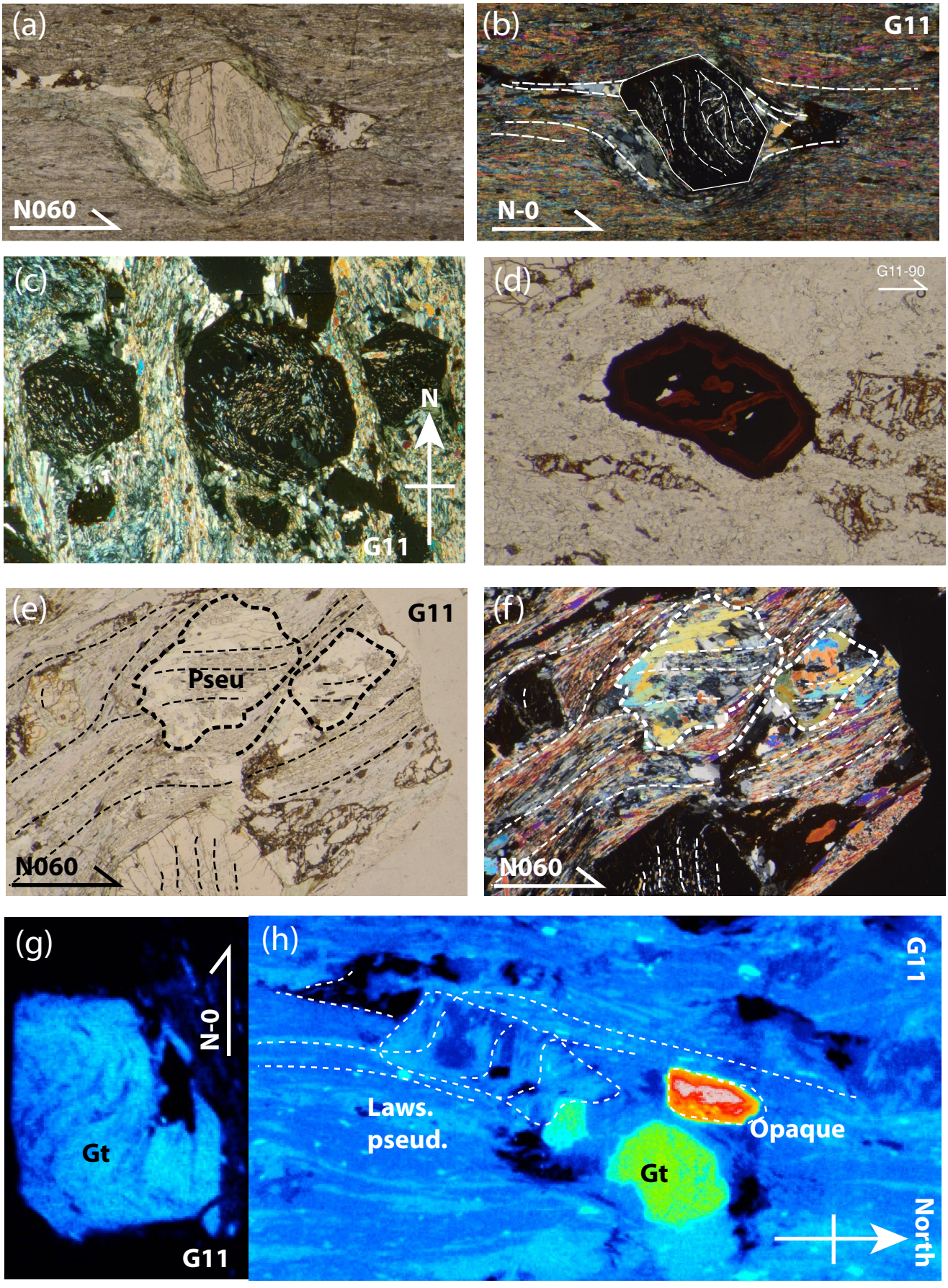
(a)
N060
(b)
G11
N-0
(c)
N
G11
(d)
G11-90
(e)
G11
Pseu
N060
(f)
N060
(g)
N-0
Gt
G11
(h)
G11
Laws.
pseud.
Opaque
Gt
North

FIG. 6

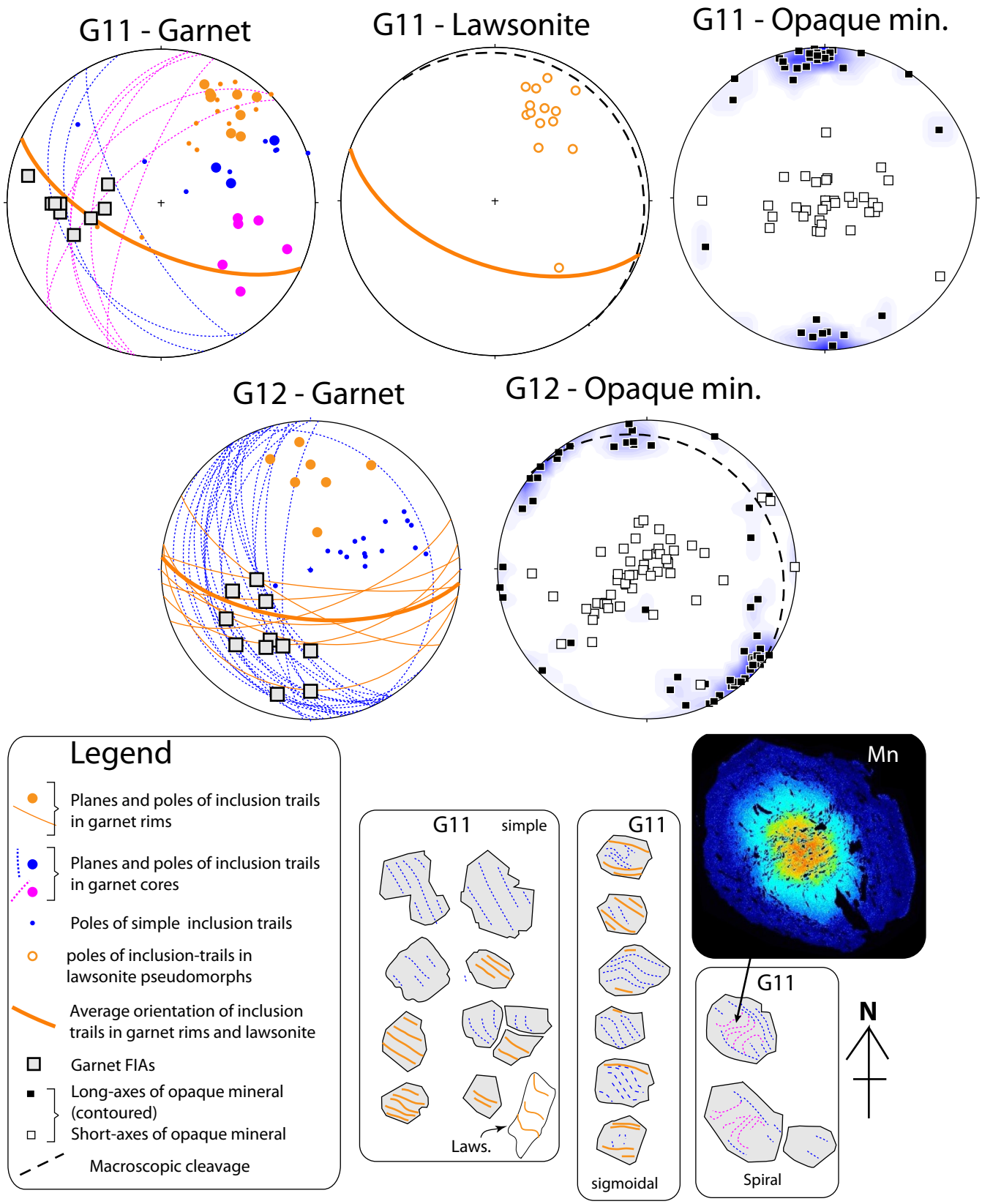
G11 - Garnet
G11 - Lawsonite
G11 - Opaque min.
G12 - Garnet
G12 - Opaque min.
Legend
Planes and poles of inclusion trails in garnet rims
Planes and poles of inclusion trails in garnet cores
Poles of simple inclusion trails
poles of inclusion-trails in lawsonite pseudomorphs
Average orientation of inclusion trails in garnet rims and lawsonite
Garnet FIAs
Long-axes of opaque mineral (contoured)
Short-axes of opaque mineral
Macroscopic cleavage
G11 simple
Laws.
G11
sigmoidal
Mn
G11
Spiral
N

FIG. 7

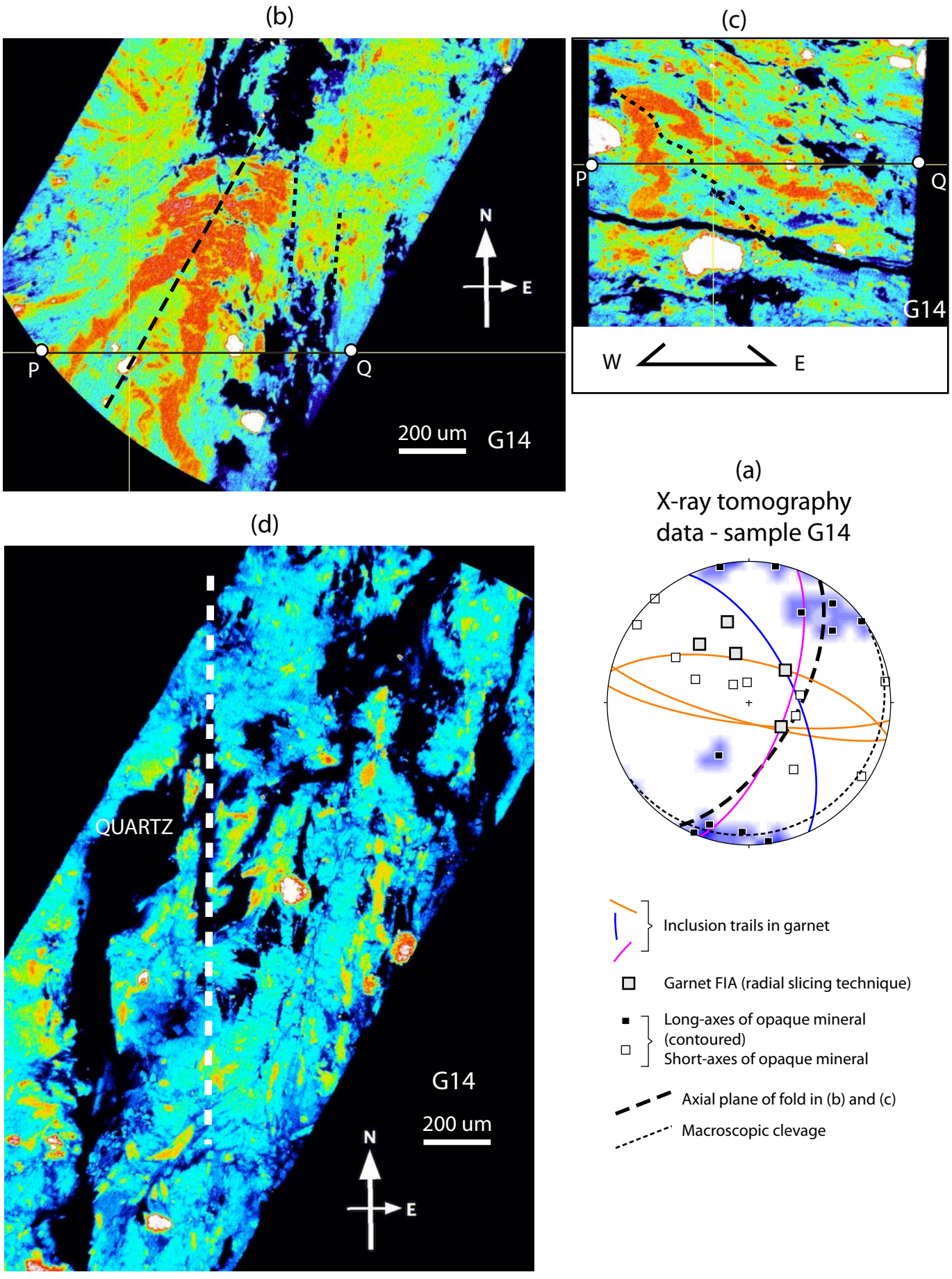
(b)
N
E
P
Q
200 um
G14
(c)
P
Q
G14
W
E
(a)
X-ray tomography
data - sample G14
Inclusion trails in garnet
Garnet FIA (radial slicing technique)
Long-axes of opaque mineral
(contoured)
Short-axes of opaque mineral
Axial plane of fold in (b) and (c)
Macroscopic clevage
(d)
QUARTZ
G14
200 um
N
E

FIG. 8

(a) Sample G3

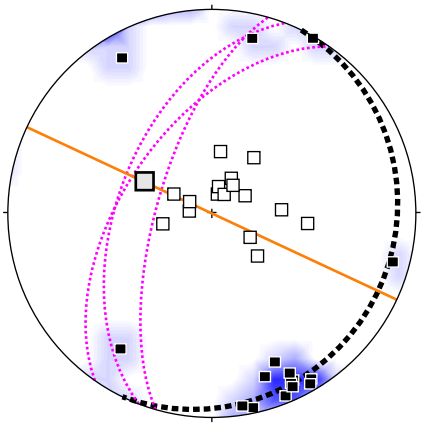

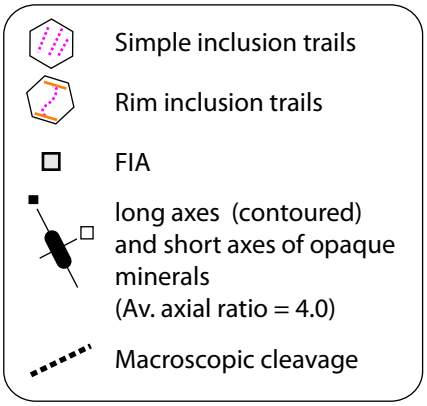

(b) Field data from Plage du Trec (C. Audren 1974)

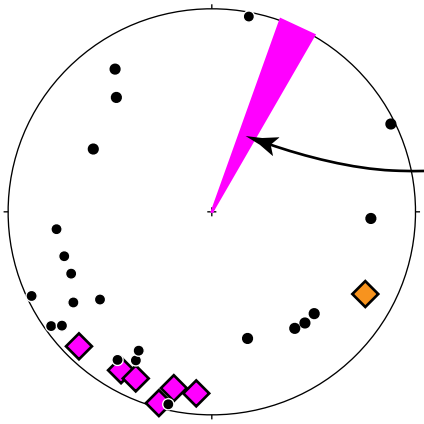

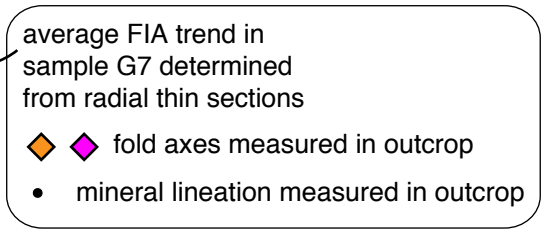

(c) Sample G20

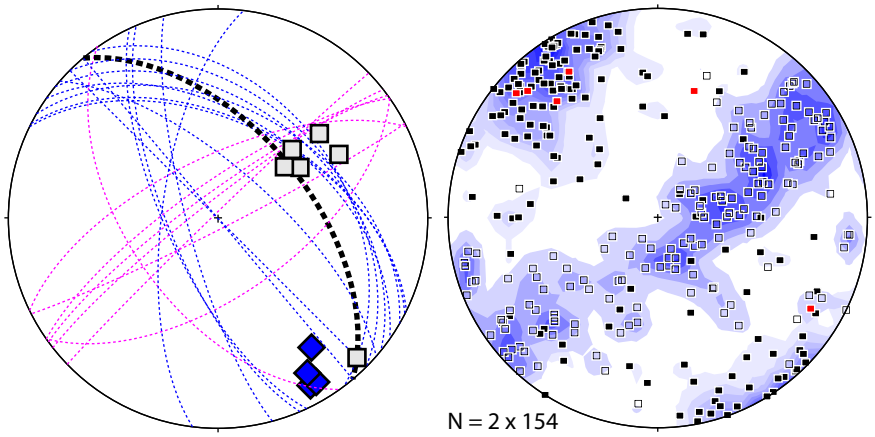

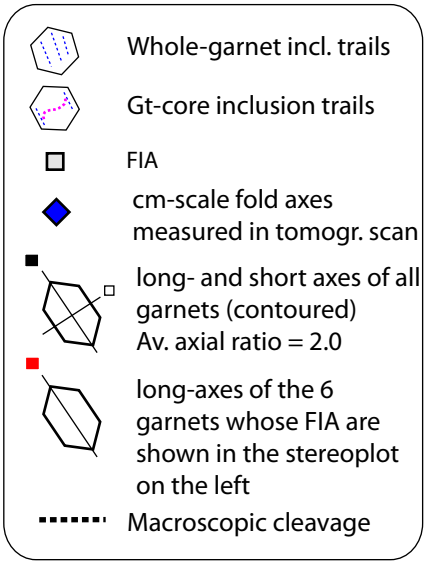

FIG. 9

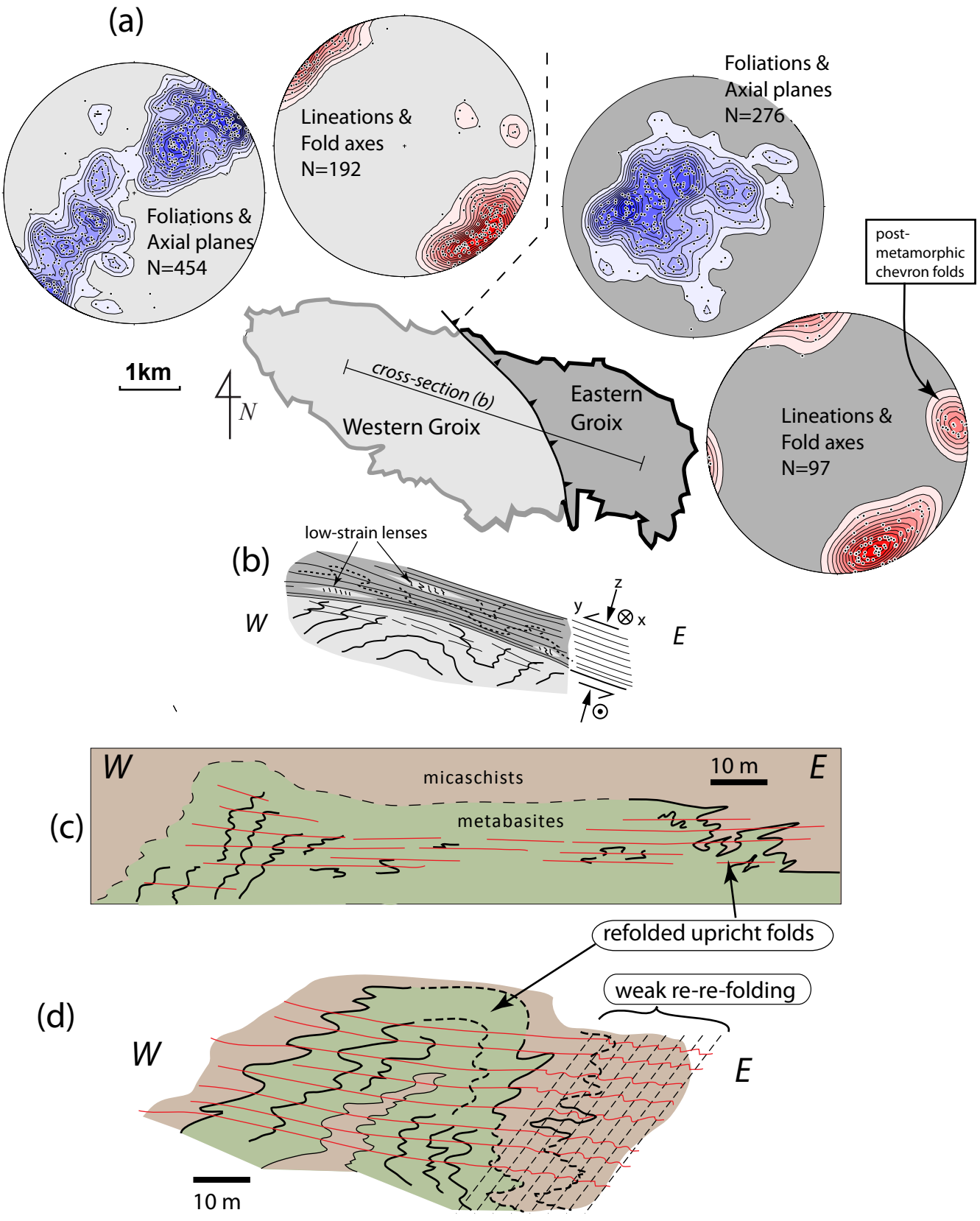
(a)
Foliations &
Axial planes
N=454
Lineations &
Fold axes
N=192
Foliations &
Axial planes
N=276
post-
metamorphic
chevron folds
Lineations &
Fold axes
N=97
1km
N
cross-section (b)
Western Groix
Eastern
Groix
(b)
low-strain lenses
W
E
z
y
x
(c)
W
micaschists
10 m
E
metabasites
refolded upricht folds
(d)
weak re-re-folding
W
E
10 m

Fig. 10

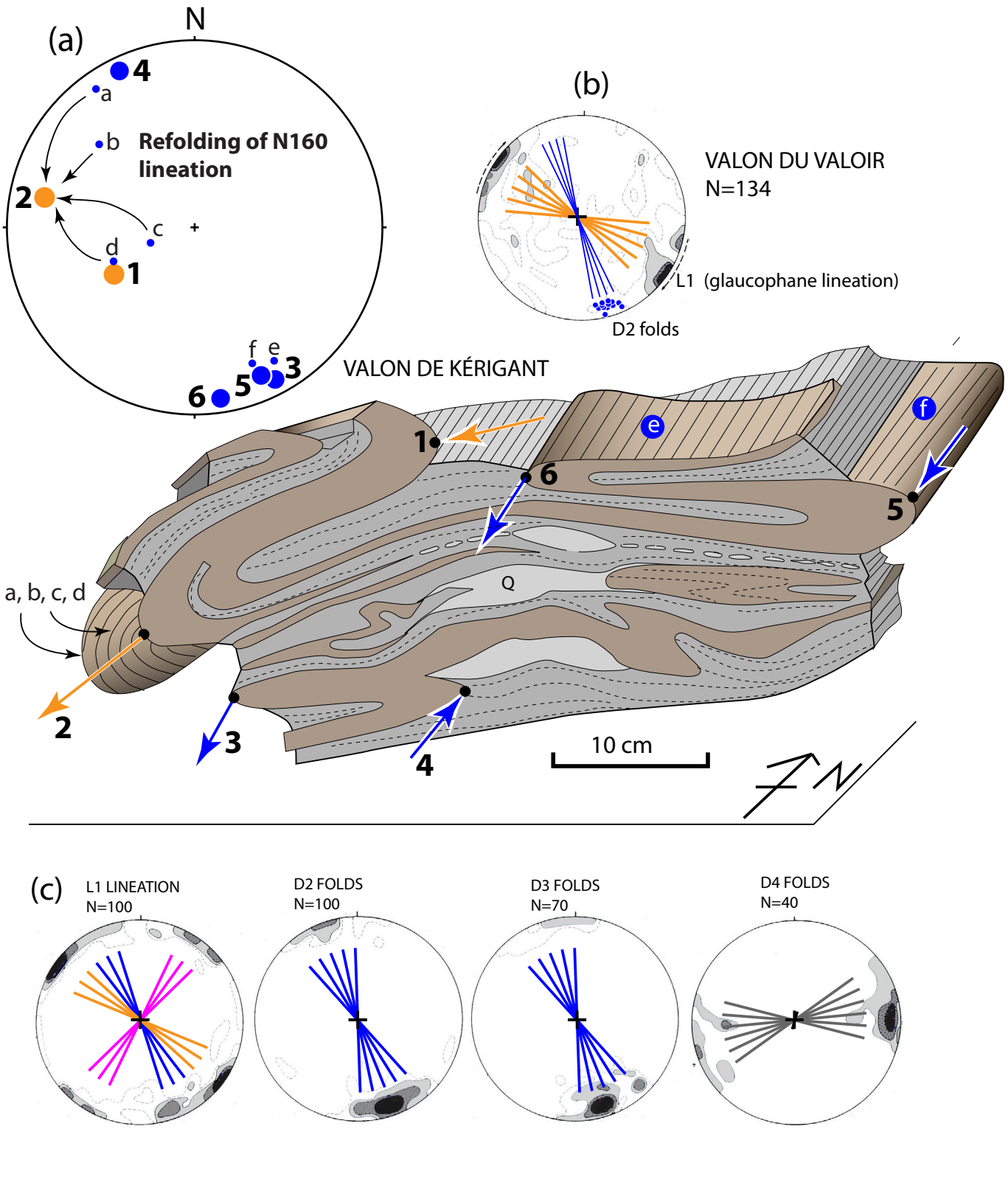
(a)
N
4
a
b
Refolding of N160 lineation
2
c
d
1
f e
3
6
5
(b)
VALON DU VALOIR
N=134
L1 (glaucophane lineation)
D2 folds
VALON DE KÉRIGANT
1
e
f
6
5
a, b, c, d
Q
2
3
4
10 cm
N
(c)
L1 LINEATION
N=100
D2 FOLDS
N=100
D3 FOLDS
N=70
D4 FOLDS
N=40

FIG. 11

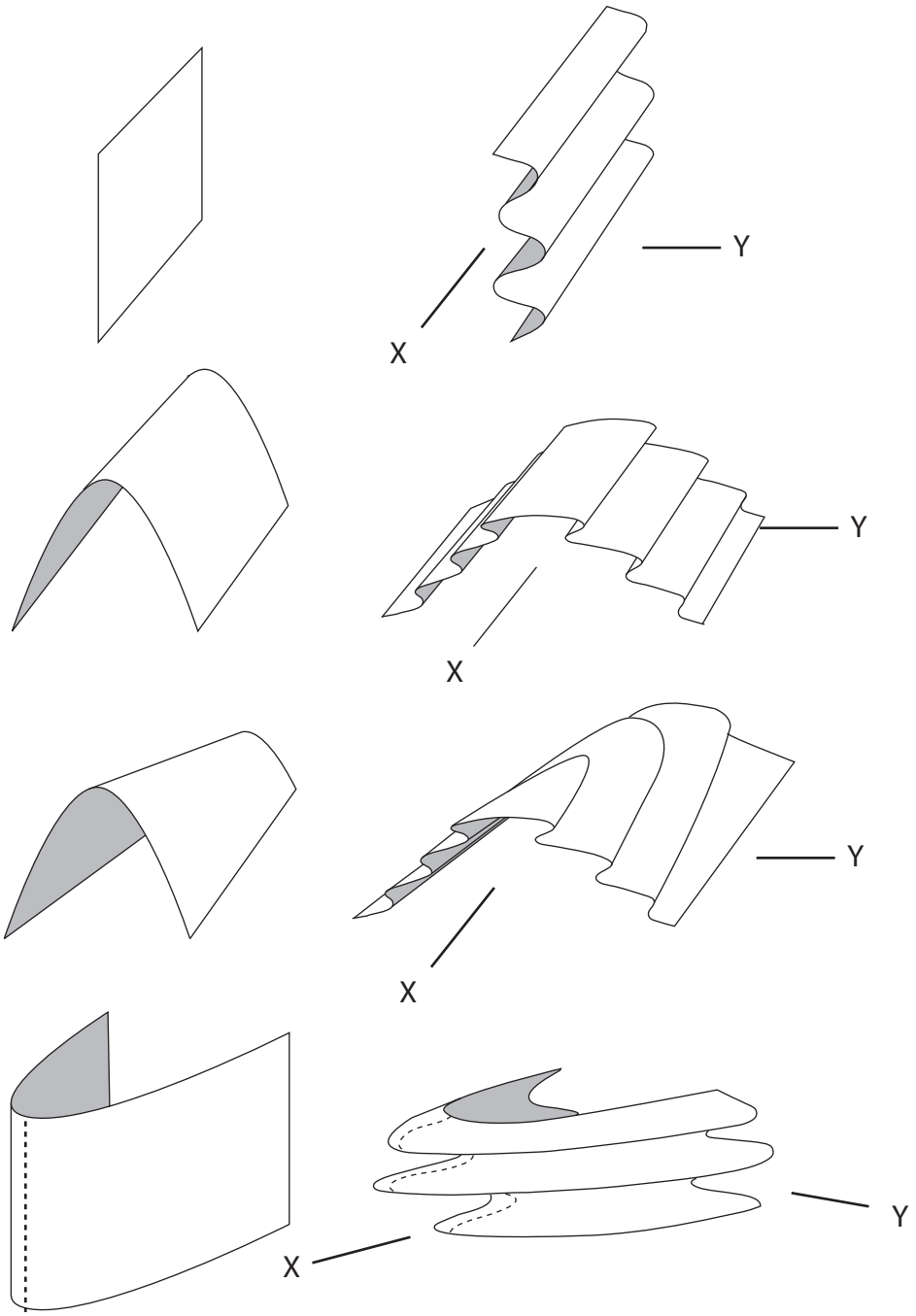

FIG. 12

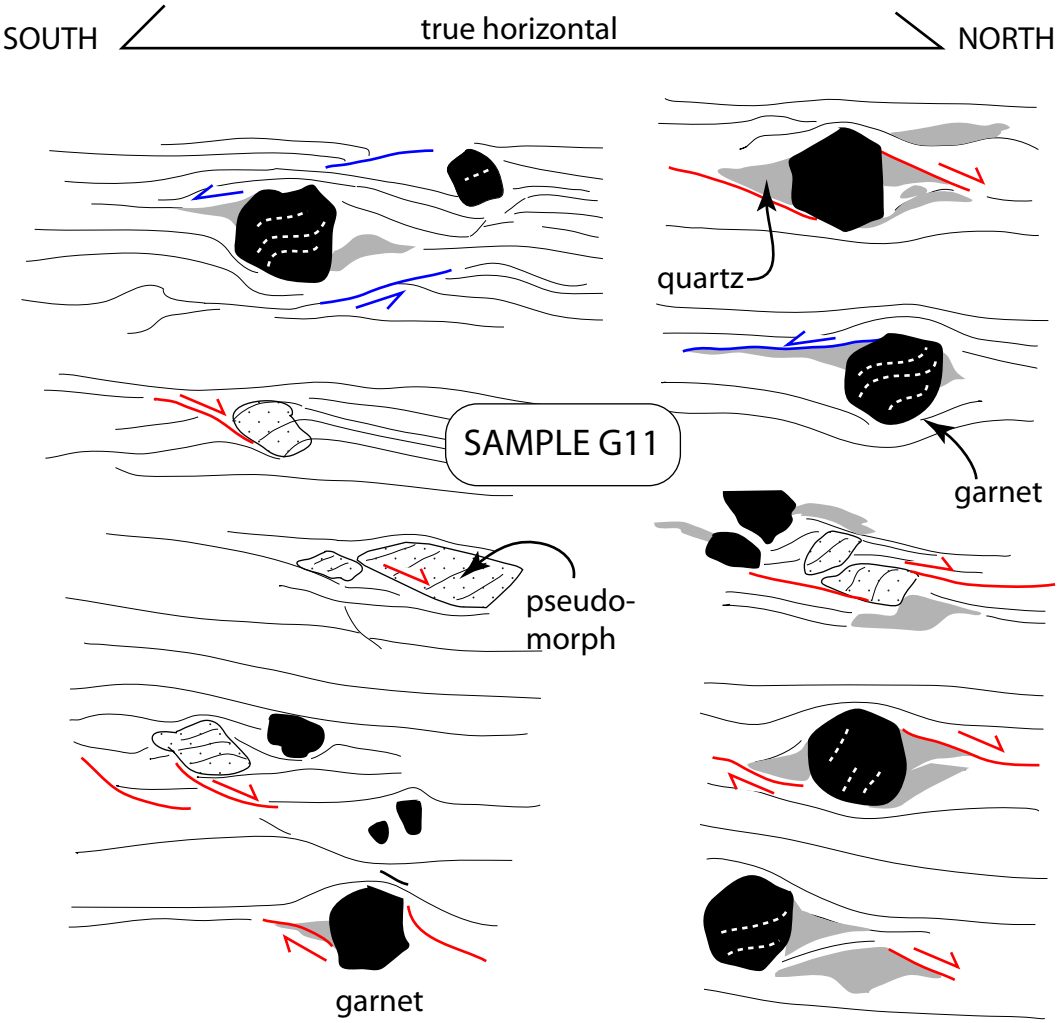
SOUTH
true horizontal
NORTH
quartz
SAMPLE G11
garnet
pseudo-
morph
garnet

Fig. 13

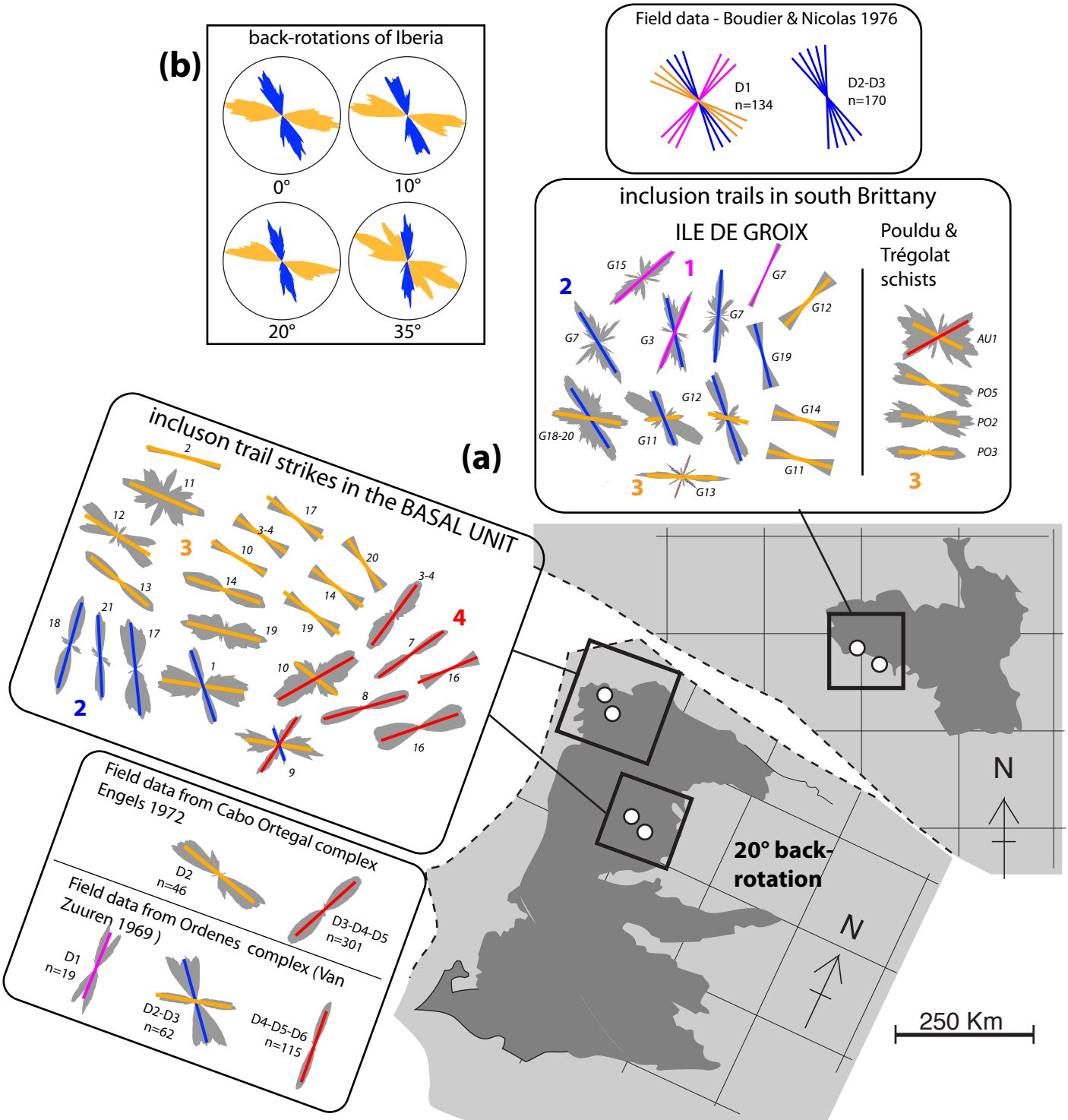
(b)
back-rotations of Iberia
0°
10°
20°
35°
Field data - Boudier & Nicolas 1976
D1
n=134
D2-D3
n=170
inclusion trails in south Brittany
ILE DE GROIX
Pouldu &
Trégolat
schists
(a)
incluson trail strikes in the BASAL UNIT
Field data from Cabo Ortegal complex
Engels 1972
D2
n=46
D3-D4-D5
n=301
Field data from Ordenes complex (Van
Zuuren 1969)
D1
n=19
D2-D3
n=62
D4-D5-D6
n=115
20° back-
rotation
N
N
250 Km

Fig. 14